Engineering Structures 317 (2024) 118647

Contents lists available at ScienceDirect

Engineering Structures

journal homepage: www.elsevier.com/locate/engstruct

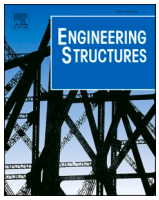

Review article

Dynamic performance of fiber-reinforced ultra-high toughness cementitious composites: A comprehensive review from materials to structural applications

Liangming Sun [a], Shuguang Liu [a], Hanbing Zhao [b,*], Umar Muhammad [a], Da Chen [b], Wengui Li [b,*]

[a] School of Civil Engineering and Architecture, Wuhan University of Technology, Hubei 430070, China
[b] Centre for Infrastructure Engineering and Safety, School of Civil and Environmental Engineering, The University of New South Wales, NSW 2052, Australia

ARTICLE INFO

Keywords:
Ultra-high toughness cementitious composites
Dynamic properties
Ductility
Fiber reinforcement
Energy dissipation ability

ABSTRACT

The durability under dynamic loading is crucial for diverse concrete structures, including buildings subjected to seismic forces as well as hydraulic and floating concrete structures in turbulent water conditions. Ultra-high-toughness cementitious composites (UHTCC) exhibit exceptional ductility, high plastic deformation capability, multiple-cracking behaviour, excellent energy dissipation, and satisfactory strength. Consequently, UHTCC holds significant promise for enhancing the resilience of concrete structures in engineering application. This study provides a comprehensive review on the dynamic properties and damage patterns of UHTCC reinforced with different fibers in various dynamic loading conditions, including unidirectional, cyclic, instantaneous penetration, and seismic loading. The material models and analysis results from numerical simulations of UHTCC are also discussed. The findings indicate that UHTCC can offer superior deformation capacity and enhanced energy dissipation properties compared to conventional concrete when subjected to dynamic excitations. The combination of steel fiber (SF) and synthetic fiber can effectively enhance the dynamic strength of UHTCC without significantly compromising its strain-hardening characteristics. UHTCC exhibits a longer service life than conventional concrete when exposed to cyclic and fatigue force. In scenarios involving projectile impacts, blast, and seismic loads, UHTCC structures maintain their integrity, thereby mitigating potential injuries. Finite element simulations of UHTCC structures necessitate highly ductile and elastoplastic material models. Future research could explore the use of more environmentally friendly fibers in UHTCC preparation and further investigate its dynamic properties at micro-level.

1. Introduction

In the past, researchers used to focus on the static properties of concrete materials. However, in most cases, concrete structures in service are subjected to dynamic loads induced by vehicle, wind, wave and even blast and projectile impact from terrorist attacks [1,2]. Researchers have recognized the significance of studying the dynamic properties of concrete structures and paid massive attention to the energy dissipation capacity of concrete materials under dynamic excitations [3]. Fig. 1(a) statistically analysed the proportion of research on static and dynamic properties of cementitious materials over the last 10 years based on the Scopus database. In the past 10 years, researchers consistently paid more attention to the dynamic properties of cementitious materials rather than their static traits, and the research on dynamic properties has shown a continuously increasing trend in the past 5 years.

The concrete material is in a coupled compression-tension state under dynamic loads [4,5]. However, its brittleness is outstanding, and microcracks within the concrete matrix expand rapidly until the collapse of the structure when subjected to compression and tensile stress waves [6]. To avoid excessive tensile force on concrete materials, engineers usually embed steel bars and hoops to enhance the overall structural tensile and shear strength. Dynamic loads would produce complicated stress waves within the concrete, in which case it is difficult to absorb the impact energy adequately by the steel reinforcement [7]. To enhance the energy dissipation capacity of cementitious composite, researchers incorporated fibers and supplementary cementitious materials (SCM)

* Corresponding authors.
E-mail addresses: hanbing.zhao@unsw.edu.au (H. Zhao), wengui.li@unsw.edu.au (W. Li).

https://doi.org/10.1016/j.engstruct.2024.118647
Received 2 March 2024; Received in revised form 25 June 2024; Accepted 16 July 2024
Available online 24 July 2024

into the plain concrete to mitigate crack distribution and restrain crack extension under dynamic loads [8,9]. Such cementitious composites with high energy consumption properties are named ultra-high-toughness cementitious composites (UHTCC), engineered cementitious composites (ECC), fiber-reinforced high ductility cementitious composites (FRHDCC) or strain-hardening cementitious composites etc. For convenience, we call it UHTCC in this study. Fibers commonly used to produce UHTCC include polyethylene (PE) fiber, polyvinyl alcohol (PVA) fiber, polypropylene (PP) fiber, poly-p-phenylene benzobisoxazole (PBO) fiber, polyoxymethylene (POM) fiber, steel fiber (SF) and basalt fiber (BF) etc [10,11]. The number of literature studies on each fiber and the corresponding UHTCC properties in the last 10 years are counted in Fig. 1(b). PVA fiber, SF and PE fiber are the three most common ones used in the preparation of UHTCC because of their easy accessibility, high tensile strength, high elastic modulus and affinity with cement matrix. Fig. 1(c) shows that the number of studies on the performance of UHTCC has continued to grow over the past 10 years. Researchers from China have published more than twice as many studies on UHTCC as the next highest-ranking countries, Germany, and the United States (see Fig. 1(d)).

UHTCC has become an emerging material that overturns the old concept of traditional cementitious materials. Benefit from the synergistic effect of fibers and composite matrix, UHTCC exhibits multiple cracking characteristics under a direct tensile load and is able to reach a tensile strain of more 3 %, which is difficult to achieve by using ordinary fiber-reinforced concrete (FRC) and ultra-high-performance concrete (UHPC) [12]. Zhu et al. [8], Yoo et al. [9], Singh et al. [10], and Shanmugasundaram et al. [11] provided a systematic and comprehensive summary of the mixture ratio design, basic mechanical properties, structural applications, and the influence of constituents on UHTCC. Fiber content, aspect ratio and mechanical properties jointly play a decisive role in the high ductility and high energy consumption of UHTCC [8]. If the fibers are too long and do not have enough tensile strength, they are prone to break under dynamic loads and cannot restrain the crack propagation [13]. Correspondingly, the strain-hardening phenomenon of UHTCC is not obvious when the tensile strength and elastic modulus of fibers are excessively high [14]. The high strength and high deformation ability of UHTCC can be achieved simultaneously by blending synthetic fibers and SF [15]. However, the damage patterns and mechanical properties of UHTCC under various dynamic loads are still inadequately summarized. A thorough understanding of the dynamic properties of UHTCC can help evaluate the potential use of UHTCC as structural primary or secondary materials [10,11].

This study systematically summarizes the crack distribution, damage sizes, peak stress, deformation capacity and energy dissipation properties of UHTCC under a series of dynamic loads. The dynamic resistance of UHTCC specimens prepared with different fibers is compared with that from plain concrete to highlight the advantages of UHTCC in dissipating impact energy and maintaining structural integrity. The ductility and strain-hardening characteristics of UHTCC at different strain rates are also summarized. Finally, new ideas are proposed for future in-depth studies on the dynamic performance of UHTCC from both micro and macro perspectives, and the possibility of enhancing the sustainability of UHTCC.

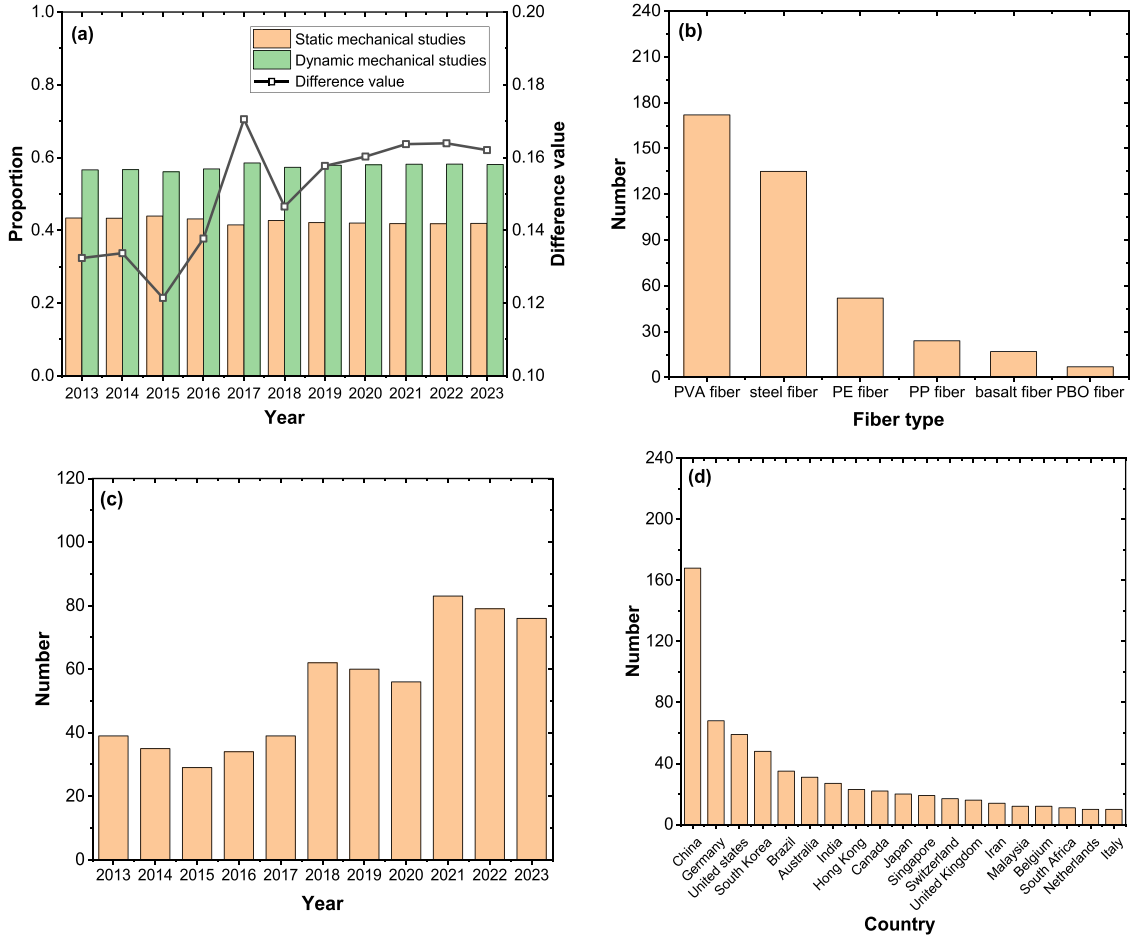

Fig. 1. Statistics on the research of UHTCC over the last 10 years based on Scopus database: (a) Relative proportion of static and dynamic research on cement-based materials; (b) Popularity of various fibers in UHTCC preparation; (c) Publications of UHTCC studies by year; (d) Publications of UHTCC studies by regions.

2. Mixture proportion design of UHTCC

The most important materials for preparing UHTCC include cement, synthetic fiber, silica sand, water, SCM and superplasticizer [10]. The cement paste matrix and fiber are designed based on micromechanical principles to achieve unique strain-hardening and multiple-cracking behaviors under a direct tensile load [11]. Therefore, UHTCC has strict requirements on the proportion of each raw material, mixing procedure and curing environments. Portland cement is the main cementitious material used in the preparation of UHTCC. Some researchers have tried to replace a part of cement with SCMs, such as fly ash, silica fume and ground-granulated blast furnace slag (GGBFS) to improve the density and durability of UHTCC [8]. However, Wishwesh and Anand [16] found that the optimal fly ash replacement ratio was only 0.25 % to improve the tensile strength and strain-hardening behavior of UHTCC. When the fly ash content reached 1 %, the tensile strength and ultimate tensile strain of UHTCC showed a downward trend [16]. Similarly, Lei et al. [17] indicated that a high volume of silica fume weakened the strain-hardening behavior of UHTCC because of fiber agglomeration and lower cohesion to fibers.

Normally speaking, higher sand to binder (S/B) ratio and lower water to binder (W/B) ratio are contributed to the improvement of direct tensile strength and fracture energy of UHTCC [11]. However, overhigh S/B ratio and excessively low W/B ratio may make it difficult for the fibers to disperse in the paste matrix, thereby weakening the tensile properties of UHTCC [11]. The fiber type, volume fraction and aspect ratio determine the bridging ability of fibers. The volume fraction of fibers is usually between 0.5 % and 2.0 %, because a large volume of fiber tends to agglomerate [8]. Ordinary synthetic fiber such as PVA fiber and PE fiber are easy to rupture instantaneously under dynamic loads, whereas SF has higher tensile strength and elastic modulus [10]. Some researchers have mixed synthetic fiber and SF as hybrid fiber and used it to fabricate UHTCC with high strength. For example, Huang et al. [18] successfully produced ultra-high-strength UHTCC with a compressive strength of more than 200 MPa and tensile strength of more than 17 MPa using 2 vol% PE fiber and 1 vol% SF. The control of temperature and humidity during the curing process also determines whether the satisfying UHTCC material can be successfully produced. It is generally believed that the ideal environment for curing UHTCC is 23 ℃ and 95 % relative humidity [11]. High temperature and low humidity will accelerate the evaporation of free water within UHTCC specimens and cause cracking. In some special cases, for example, Huang et al. [18] and Lao et al. [19] used water tank curing method and plastic film covering method to cure UHTCC specimens at 80–90 ℃ to accelerate the pozzolanic reaction speed of fly ash and achieved ultra-high-strength or high-strength UHTCC materials.

3. Mechanical performance of UHTCC under unidirectional dynamic loads

3.1. Dynamic compression load

Researchers usually apply impact loads to materials using a Split-Hopkinson Pressure Bar (SHPB) [20]. The impact load created by SHPB device is different from drop weight load and projectile impact. The end of SHPB incident bar is a circular plane with a diameter of 80 mm or 100 mm, which can apply uniform and stable compressive force at a high strain rate [21]. Stress-strain curves of concrete specimens under impact load can be obtained by SHPB device, which provides essential information for exploring the relationship between strain rate and mechanical properties of UHTCC [21].

Fig. 2 shows the stress-strain curves of UHTCC specimens reinforced by different types of synthetic fibers subjected to dynamic compression loads at a strain rate of about 105 s^{-1}. It can be clearly seen that compared to the cement mortar counterparts under impacts of 110 s^{-1}, the peak strain was increased, and the post-peak ductility was

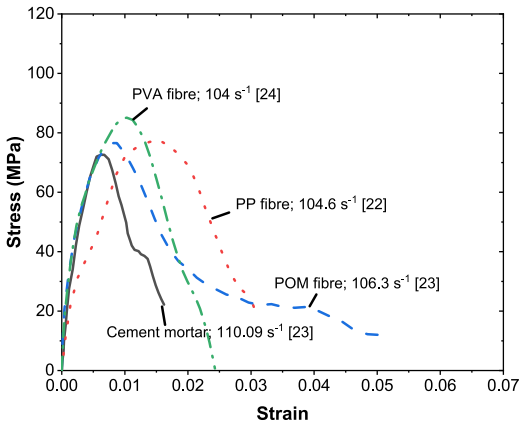

Fig. 2. Dynamic compression stress-strain curves of cementitious composites with traditional synthetic fibers [25–27].

significantly enhanced for UHTCC. Specifically speaking, the peak strain of UHTCC reinforced by PP fiber can reach approximate 0.015. In addition, the ultimate strain of UHTCC reinforced by POM fiber can reach over 0.05. However, the corresponding values of ordinary cement mortar were only 0.006 and 0.016 respectively. Kai et al. [22] obtained stress-strain curves of UHTCC specimens containing 2 % PVA fibers under strain rates from 96 s^{-1} to 197 s^{-1}. The increasing ratio of dynamic increase factor (DIF, the ratio of the dynamic compressive strength to the quasi-static strength) was about 1.4, higher than 1.1 of conventional concrete. This indicates that UHTCC reinforced by PVA fiber possesses a more significant resistance ability to impacts. However, Kai et al. [22] drew up the above conclusions about UHTCC mainly by referring to the test data of conventional concrete provided by other researchers, without designing a reference group in their experiments. Zhao et al. [23] compared the dynamic compressive behavior of UHTCC under dry and wet states. They reported that the dynamic compressive strength and specific energy absorption of UHTCC under a dry state were higher than those from conventional cement mortar because of the fiber bridge effect. However, PVA fiber was more likely to be pulled out rather than ruptured under wet conditions because free water weakened the cohesion strength of PVA fiber with cement paste [23]. Nanomaterials can improve pre-peak stiffness and post-peak ductility of UHTCC under high strain rate [24]. In Chen et al.'s research [24], 2 % nano silica (NS), nano titanium dioxide (NT) and nano calcium carbonate (NC) by mass of cementitious material can slightly improve the mechanical properties and strain rate sensitivity of UHTCC under dynamic compression load. However, the micro-level evidence and explanations provided for these differences were insufficient.

PE and PVA fibers are usually used as reinforcements to improve the ductility of UHTCC because of their relatively low modulus and satisfactory tensile strength [28]. During these years, many researchers have devoted themselves to finding alternatives to replace traditional PE and PVA fibers. For example, BF, SF and hybrid fiber have been attempted to in the preparation of UHTCC [28,29]. SF possesses better physical and mechanical properties than traditional synthetic fibers, especially its elastic modulus (about 200 GPa) is obviously higher than that of PE fiber (about 66 GPa) and PVA fiber (40 GPa) [30,31]. In Li et al.'s research [30], UHTCC with 1.5 % volume fraction of SF and 2.0 % volume fraction of PVA fiber exhibited better dynamic behaviour than SF reinforced concrete and UHTCC with only PVA fiber. Similar to SF, BF can also improve the dynamic compression performance of UHTCC [32]. However, the elastic modulus of SF and BF are excessively high, which enhance the dynamic compressive strength at the expense of the strain-hardening ability of UHTCC [28,32]. The static tensile strain capacity of UHTCC made with BF in Zhang et al.'s research [28,32] was only 0.5 %. Similarly, the static tensile strain capacity of SF cementitious composites was only about 1.0 % [20]. Therefore, it is difficult to

prepare UHTCC with solely these two fibers to achieve a strain-hardening capacity of over 3 % that is routinely perceived to be desirable [29,33]. As a result, researchers usually apply them in conjunction with conventional synthetic fibers to meet both dynamic compressive strength and tensile ductility requirements [29,33,34].

3.2. Dynamic tensile load

The most prominent feature of UHTCC is its significant pseudo-strain hardening behaviour under direct tensile load [35]. Therefore, the energy absorption capacity of UHTCC is much higher than those from ordinary concrete and normal fiber-reinforced concrete [36]. The advantages of UHTCC in high ductility and high toughness are outstanding when subjected to dynamic loads [37,38]. However, most of known mechanical properties of UHTCC come from quasi-static tensile experiments. The strain rate has a significant impact on the tensile properties of UHTCC, and a constant strain rate during dynamic tensile tests can be achieved by adjusting the loading velocity of the direct tensile machine [39,40].

The tensile stress-strain curves of UHTCC made with PVA fiber in Fig. 3 disclose the strain rate effect on the tensile properties of UHTCC. Under quasi-static tensile load (strain rate=3.7 $\times 10^{-5}$ s^{-1}), UHTCC specimens showed obvious strain hardening trait [41]. Specifically, the ultimate tensile strain exceeded 4.5 % without significant decrease in tensile strength [41]. As the strain rate increased, the tensile strain capacity of UHTCC decreased gradually, whereas the strength was improved [41]. When the tensile strain rate reached 3.7 $\times$ 10^{-1} s^{-1}, the strength of UHTCC was increased to nearly 5 MPa [41]. Correspondingly, the ultimate tensile strain was only one-fifth of that under quasi-static tension [41].

To obtain a higher strain rate, Hou et al. [37] installed a drop hammer system based on traditional static tensile test equipment to provide an instantaneous tensile load with high strain rate for UHTCC dumbbell specimens through the gravitational potential energy of the drop hammer. The test results of Huo et al. [37] are similar to the conclusions in the low strain rate. The tensile strain capacity of UHTCC decreased while the tensile strength increased with the rising of impact height [37].

Although Huo et al. [37] successfully applied direct tensile load with high strain rate on UHTCC dumbbell specimens, this dynamic tensile load was transient and unstable. Li et al. [39] used a professional high-speed servo control dynamic tensile apparatus to apply a sustainable and stable dynamic tensile load with a strain rate of 90.01 s^{-1}. The test results of UHTCC made with PVA fiber are shown in Fig. 4. It can be seen that when the strain rate was between 0.9 s^{-1} and 9.71 s^{-1}, the stress-strain curve was approximately consistent with the findings in

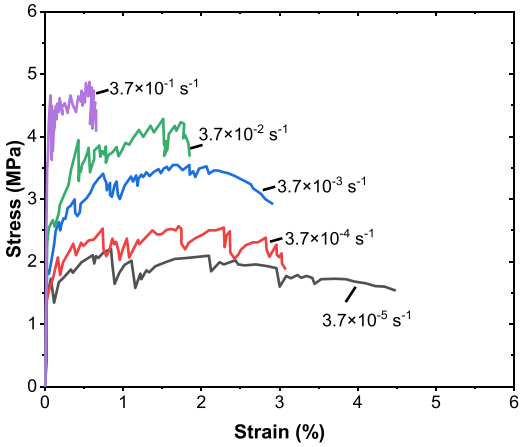

Fig. 3. Stress-strain curves of PVA fiber reinforced UHTCC under dynamic direct tension [41].

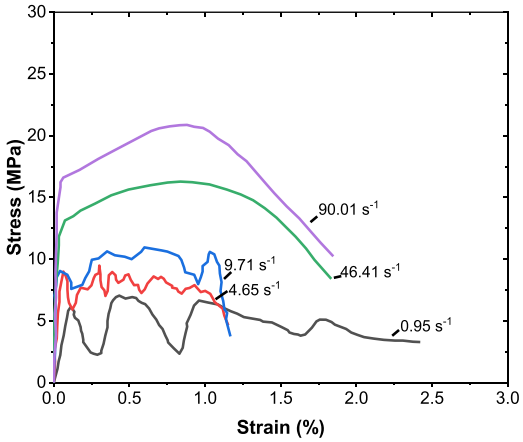

Fig. 4. Stress-strain curves of UHTCC under dynamic tensile loads at high strain rates [39].

Fig. 3 [39]. However, when the strain rate reached 46.41 s^{-1} and 90.01 s^{-1}, the trend of stress-strain curves changed obviously [39]. The pseudo-strain hardening plateau disappeared, and UHTCC specimens exhibited more brittle failure characteristics similar to those under dynamic compression [39].

Fig. 5 shows the typical failure patterns of UHTCC dumbbell specimens made with PE fiber under quasi-static and dynamic tensile loads [42]. Due to the bridge effect of PE fiber, multiple cracks appeared on the surface of the UHTCC specimen [42]. The development process of cracks corresponds to the strain-hardening part in the stress-strain curve. When the strain rate was raised, the number and width of cracks decreased because high strain rates increased the probability of fiber fracture, resulting in the bridging effect not being fully utilized [43,44].

Researchers usually use the thermo-activated mechanism to explain the strain rate effect under dynamic compression [45]. The thermo-activated mechanism suggests that the energy required to create new cracks in a concrete specimen is higher than the propagation of old cracks [45]. As shown in Fig. 6(a), at high strain rates, the energy within the concrete specimen has no time to dissipate [45]. As a result, a large number of new cracks parallel to dynamic compression loads will be generated and then destroy the specimen [45]. This can be verified by the severe fragmentation failure mode of concrete specimens under high strain rate dynamic compression. However, this theory fails to well explain the strain rate effect of UHTCC under dynamic direct tensile load, because many studies found that dynamic tensile stress tends not to propagate uniformly in dumbbell specimens, thus leading to a

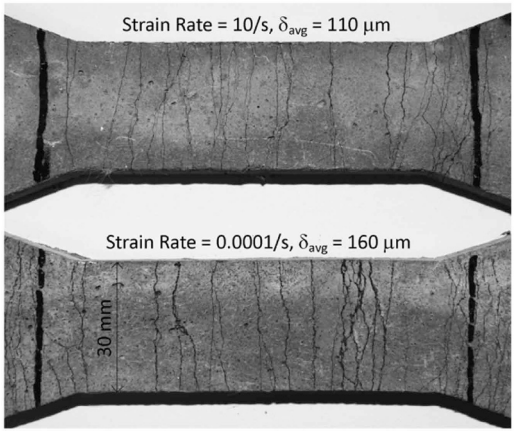

Fig. 5. Failure patterns of UHTCC under different strain rates of direct tensile load [42].

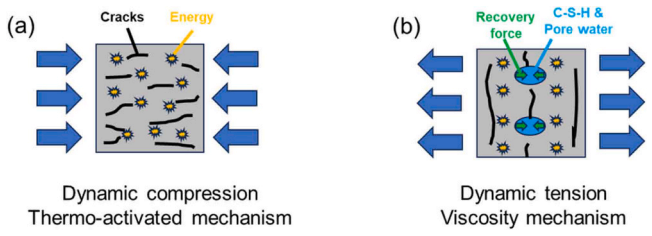

Fig. 6. The schematic diagrams of UHTCC failure mechanism under dynamic loads.

decrease in the number of cracks in concrete specimens [39,43]. Instead, the viscosity mechanism gives a better explanation [39,43]. The viscosity mechanism regards the free water and Calcium Silicate Hydrate (C-S-H) gel in concrete as a viscous liquid as shown in Fig. 6(b). When the particles in concrete are separated by a high strain rate dynamic load, the viscous liquid will provide a recovery force for particles. This additional recovery force increases the dynamic tensile strength of concrete, and the cracks perpendicular to dynamic tensile loads are generated on the specimen. In addition, the inertia mechanism can also be used to explain the mechanical performance of UHTCC under dynamic tensile load [46–49]. The inertial effect of the solid particles within the UHTCC under high-speed loading provides additional spurious strength to specimens [46,50].

When concrete slabs and beams are subjected to explosion or impact loads, their free rear surfaces will instantly produce tensile stress with a strain rate of more than 10 s^{-1} [51]. However, it is difficult for direct tensile experiments to achieve a strain rate exceeding 1 s^{-1}. Only Ranade et al. [42] and Li et al. [39] achieved this strain rate requirement through special equipment in their experiments. Most importantly, it is difficult to avoid load eccentricity and uneven deformation of dumbbell specimens in direct tensile tests, especially at high strain rates [45]. The SHPB system is a common machine used to test the impact mechanical properties of concrete materials. The dynamic splitting tensile properties of UHTCC can be obtained by adjusting the loading direction of Brazilians disc specimens so that the diameter direction is subjected to impact loads [52,53]. Fig. 7 shows the stress-strain curves of SF and PE fiber reinforced UHTCC under splitting tensile impact loads.

Zhao et al. [51,52] used the above method and tested the dynamic splitting tensile strength of UHTCC containing PVA fiber and SF. The results are similar to those of the dynamic direct tensile tests at low strain rates, but the increase rate in tensile strength decreased at high strain rates [51,52]. For example, when the strain rate was 4.7–6.3 s^{-1}, the splitting tensile strength increased by 30.9–59.3 % compared to the quasi-static state, whereas the growth ratio decreased to 10.8–22.3 % when the strain rate increased from 4.7–6.3 s^{-1} to 9.9–11.0 s^{-1} [51,52]. Gong et al. [54] obtained similar conclusions using digital image correlation (DIC) technique to observe the crack development pattern of carbon textile and short polymer hybrid fiber UHTCC under impact tensile load. Several peak stresses appeared in the test data, and the DIF of peak stress corresponding to the initial crack was always the largest, because inertia plays an important role [54].

SHPB splitting tensile tests have some limitations. For example, it is difficult to observe the unique multi-crack behavior of UHTCC in split tensile experiments [53,55]. However, the width and number of cracks determine the strain-hardening capacity of the composite [53,55]. Park et al. [56] used an improved strain energy frame impact machine (I-SEFIM) to apply dynamic tensile loads with strain rates of up to 161 s^{-1} on UHTCC bell-shaped specimens. They found that SF can effectively improve the dynamic tensile strength of the composite [56]. However, equally important properties such as ultimate tensile strain capacity and energy absorption capacity are jointly affected by the matrix, fiber and fiber-matrix interface [56]. Simply increasing the volume fraction of SF would greatly raise the material cost without improving the strain and energy absorption capacities of UHTCC at high strain rates [56]. Pyo and El-Tawil [53] established a finite element model of modified strain energy frame impact machine (M-SEFIM). Simulation and experimental results show that peak stress, strain capacity and strain dissipation capacity were all significantly influenced by strain rate variations [53].

3.3. Dynamic flexural load

Flexural strength and the corresponding deformation capacity are important indicators for evaluating concrete beams. Fig. 8 shows the flexural load-crack width curves of UHTCC beams under dynamic flexural loads. Under the high strain rate, the ductility of UHTCC beam reduced obviously, but the specimen can withstand higher flexural loads [57]. Ismail et al. [58] tested the flexural performance of UHTCC beams reinforced by different fibers under impact loading. They found that those composite specimens could withstand more impact flexural loads than ordinary concrete beams [58]. The UHTCC beam reinforced by SF can maintain its integrity after being subjected to 1463 times of ACI impact loads (ACI Committee 544), whereas the UHTCC with PE and PVA fiber broke in half under the same loads, indicating that SF has a better bridging effect and stitching action [58]. For UHTCC beams with initial fracture, Gao et al. [57] found that as strain rate increased from

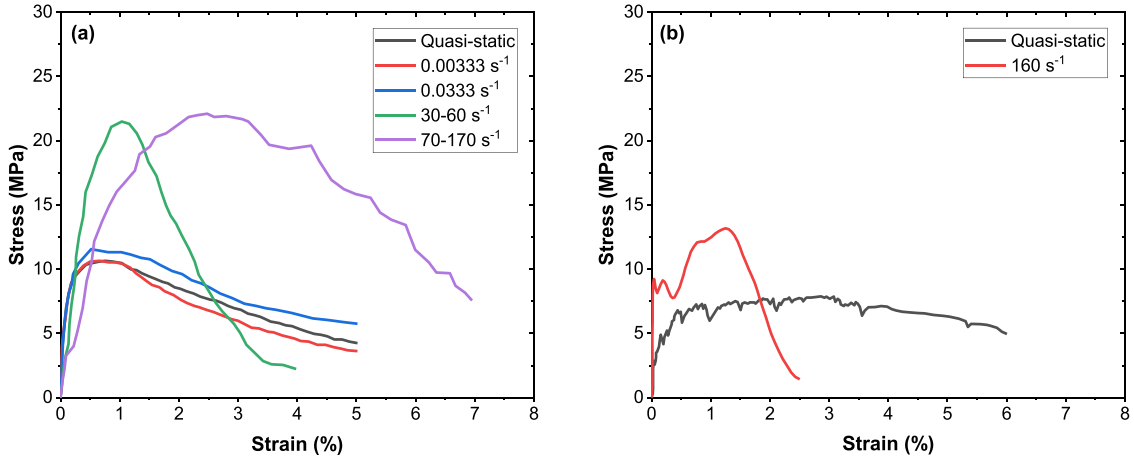

(a) Steel fiber [54] (b) PE fiber [55]

Fig. 7. Stress-strain curves of UHTCC under impact tension.

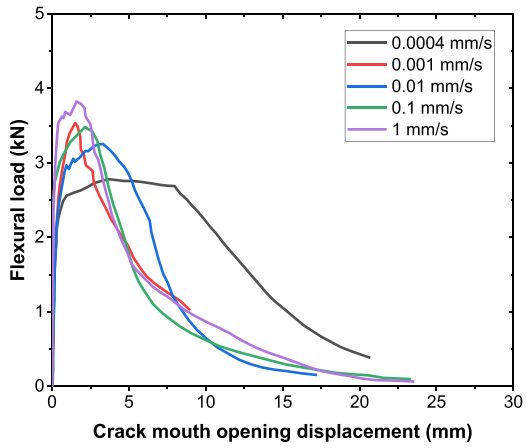

Fig. 8. Dynamic flexural properties of PVA fiber reinforced UHTCC at various strain rates [57].

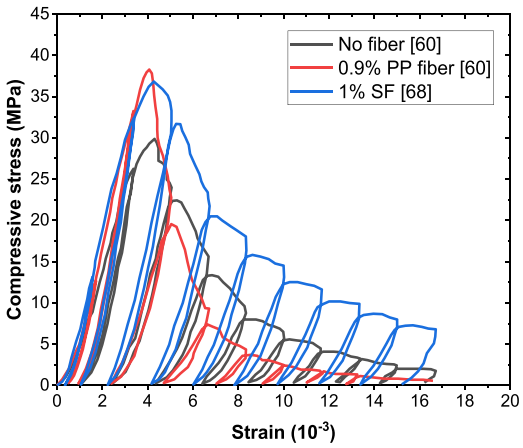

Fig. 9. Stress-strain curves of UHTCC under cyclic compression load.

0.0004 mm/s to 1 mm/s, the initial cracking load increased by 57.6 %, the peak load rose by 46.5 %, and the fracture energy decreased by 20.8 %. Hou et al. [59] used numerical simulations to apply an impact flexural load to the UHTCC rectangular plate reinforced by 2 % PVA fiber. They hypothesized that fibers would provide bridging force and dissipate energy at cracks [59]. Therefore, as the curing age of specimens increased, the fiber-matrix bonding strength enhanced to an idea value, and UHTCC exhibits more obvious multiple cracking behaviour under the same impact load [59].

4. Dynamic performance of UHTCC under cyclic loads

4.1. Low-frequency cyclic load

Fiber-reinforced UHTCC has better energy dissipation capacity than traditional concrete and UHPC, so it can still maintain good integrity under impact loads [60,61]. However, the damage within the UHTCC may gradually accumulate under cyclic loads and cause the UHTCC structure to collapse during long-term service [62–64]. Investigating the mechanical performance of UHTCC under cyclic loading can help evaluate its long-term performance.

Each compression cycle on UHTCC specimens is accompanied by elastic and plastic strains [65]. In the rising branch of the stress-strain curve, the UHTCC is dominated by elastic deformation, so the specimen can almost return to its original state upon unloading [65,66]. However, as the number of compression cycles increased, the compressive stress of the envelop curve reached a peak value and significant residual deformation occurred after unloading, which is due to the gradual accumulation of damage within the composite [67]. In addition, the hysteresis appeared, that is the reloading ascent curve can no longer follow the previous unloading curve because the cracks within the UHTCC expanded, whereas the remaining intact matrix can provide elastic deformation for the next compression [68]. In the last few cycles, the elastic deformation part of the stress-strain curve shortens and the post-peak curve becomes gentler [68].

Cyclic compression stress-strain curves of UHTCC and ordinary concrete are shown in Fig. 9. It can be seen that 0.9 % PP fiber and 1 % SF can effectively restrain the crack extension and improve the peak compressive stress. The descending section of the stress-strain curve for SF reinforced UHTCC is much flatter, indicating that SF still has a satisfying bridge effect when the cracking width expands to a large value. In contrast, the slope of the descending segment of the stress-strain curve for 0.9 % PP fiber-reinforced UHTCC is greater than that of ordinary concrete. The tensile strength of the PP fiber used in Wu et al.'s research [60] is only 400 MPa, which is much lower than that of SF, normally over 1000 MPa. During cyclic compression, the increasing crack width leads to fracture of some PP fibers, which results in more brittle damage characteristics after the stress-strain curve reaches the peak point [60]. Wang et al. [64] adopted high quality PP fibers with tensile strength over 550 MPa. Based on the envelop curves, Wang et al. [64] indicated that increasing the volume fraction of PP fiber can reduce the slope of the descending section of the stress-strain curve. However, excessively increasing the content of the fiber could make them difficult to disperse evenly during the mixing process, which may have a negative impact on the strength and ductility of concrete [64,69,70].

Tensile stress is more sensitive to microcracks [71]. As a result, the elastic deformation of the concrete materials is limited in tension [62,71]. As shown in Fig. 10, the UHTCC specimens were accompanied by obvious residual strains after each tensile cycle, and the residual strains gradually increased in the last few cycles as internal damage accumulated. Another difference with the cyclic compression stress-strain curve is that the unloading and reloading branches of each cycle almost overlap, because there is almost no elastic deformation under tensile stress for UHTCC specimens [62,71]. This also demonstrates the generation of numerous microcracks within the UHTCC after the first tensile cycle and the gradual expansion of these cracks in subsequent cycles without creating new cracks in the remaining intact matrix [62]. In addition, according to Fig. 10 (a) and (b), the increase in the volume fraction of SF from 1 % to 2 % does not significantly enhance the peak tensile stress of UHTCC. As per the above explanation, tensile stress can capture microcracks within the UHTCC and promote the expansion of these microcracks in subsequent cycles. It should be noted that a higher amount of SF increased the volume fraction of interfacial transition zone (ITZ) between SF and paste matrix [68]. ITZ is usually considered as a collection of pores and cracks in the concrete material, and the contribution of excess SF to the improvement of bridge effect becomes negligible [67,68]. The increase in peak tensile stress to 7 MPa for UHTCC specimens containing 3 % SF is mainly due to the effect of the mixture proportion differences [63].

The UHTCC beam can be divided into an upper compression part and a lower tension part under cyclic flexural load [67]. It can therefore be seen as a combination of cyclic compression and cyclic tension. The peak flexural load of 2 % SF-reinforced UHTCC was significantly improved compared to 1 % SF-reinforced UHTCC, shown in Fig. 11. In addition, the higher content of SF also increased the area of the hysteretic loops, indicating a better energy dissipation capacity [72]. However, on the other hand, the degradation process of UHTCC beams containing 2 % SF was more rapid under cyclic bending loads. After flexural cycles with a displacement of 0.5 mm, the bending load of the UHTCC containing 1 % SF decreased from the peak value of 92.1 kN to 13.7 kN in the 10th cycle, with a decrease of 78.4 kN, whereas the bending load of the UHTCC containing 2 % SF decreased from the peak value of 135.8 kN to 29.3 kN in the 10th cycle, with a decrease of 106.5 kN. This is because

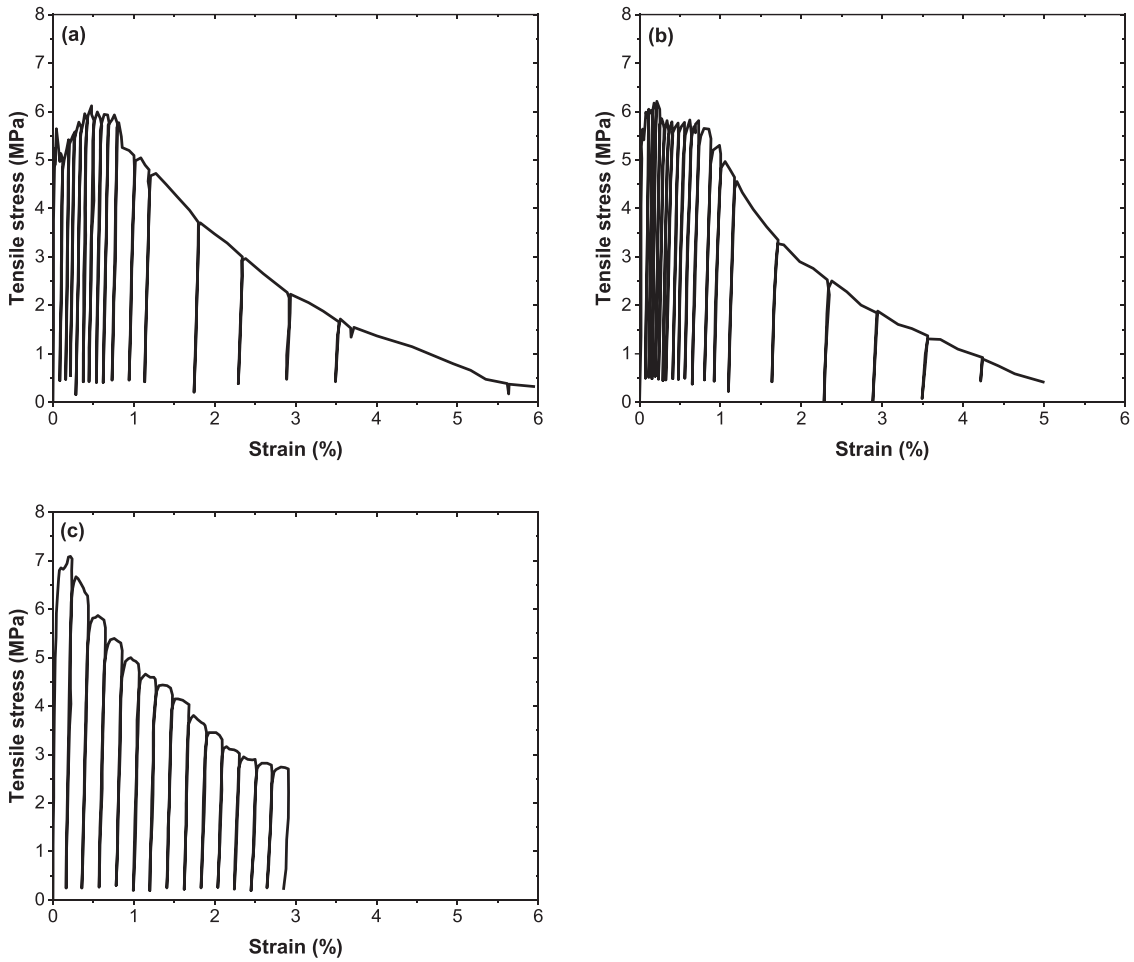

Fig. 10. Stress-strain curves of UHTCC under cyclic tensile load: (a) 1 % SF [61]; (b) 2 % SF [61]; (c) 3 % SF [63].

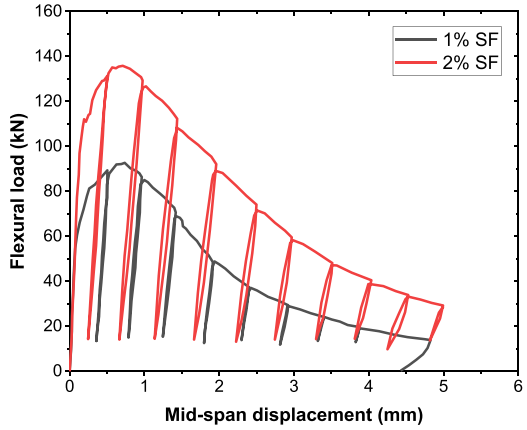

Fig. 11. Load-displacement curves of UHTCC under cyclic bending load [61].

the excessive SF improved the volume fraction of weak regions in the matrix of UHTCC [72,73].

4.2. *High-frequency fatigue load*

The repeated loading with higher frequency and longer duration can be defined as high-frequency fatigue load. Concrete structures exposed to machine- and vehicle-induced vibration over the years can suffer from significant damages caused by fatigue loading [74]. Similar to the principle of ordinary cyclic loading, fatigue loading eventually leads to structural failure by gradually expanding the initial damage within the concrete [75]. The bridge effect of fibers on microcracks within concrete remains positive under fatigue loading [75,76].

The fibers on the failure surface of UHTCC subjected to static compression show both rupture and pull-out patterns, as shown in Fig. 12 (a), whereas the pattern is different when subjected to fatigue loads [77]. As shown in Fig. 12 (b) dark areas marked by dashed lines appeared on the failure surface of the UHTCC specimen under fatigue compression. It can be observed from SEM images that these regions are the initial failure surfaces of the UHTCC in the early stage of fatigue compression, and the friction traces were remained in the subsequent repeating load [77]. PVA fiber ends within these regions were crushed in grinding and friction [77,78].

In fact, the composite matrix and fibers at the failure surface would not always exhibit grinding and friction state during the whole fatigue damage progress [78]. Li et al. [78] divided the fatigue compression damage process of PVA fiber reinforced UHTCC into three stages, as shown in Fig. 13. In the stage I, the fatigue deformation increased rapidly and microcracks were generated inside the UHTCC specimens [78]. Subsequently, the bridge effect of PVA fibers takes effect and the UHTCC specimen enters a deformation stabilization period where the fibers rupture or is pull-out [78,79]. At the end of stage II, most of the PVA fibers fail and the fiber ends that are on the friction traces are ground and crushed [78]. In the stage III, the cracks on the failure surface expand rapidly with a significant increase in deformation [78,80]. The additional fracture surface in stage III expands throughout the specimen in the last few cycles, and the fibers showed a rapture and pull-out modes in these new regions [78].

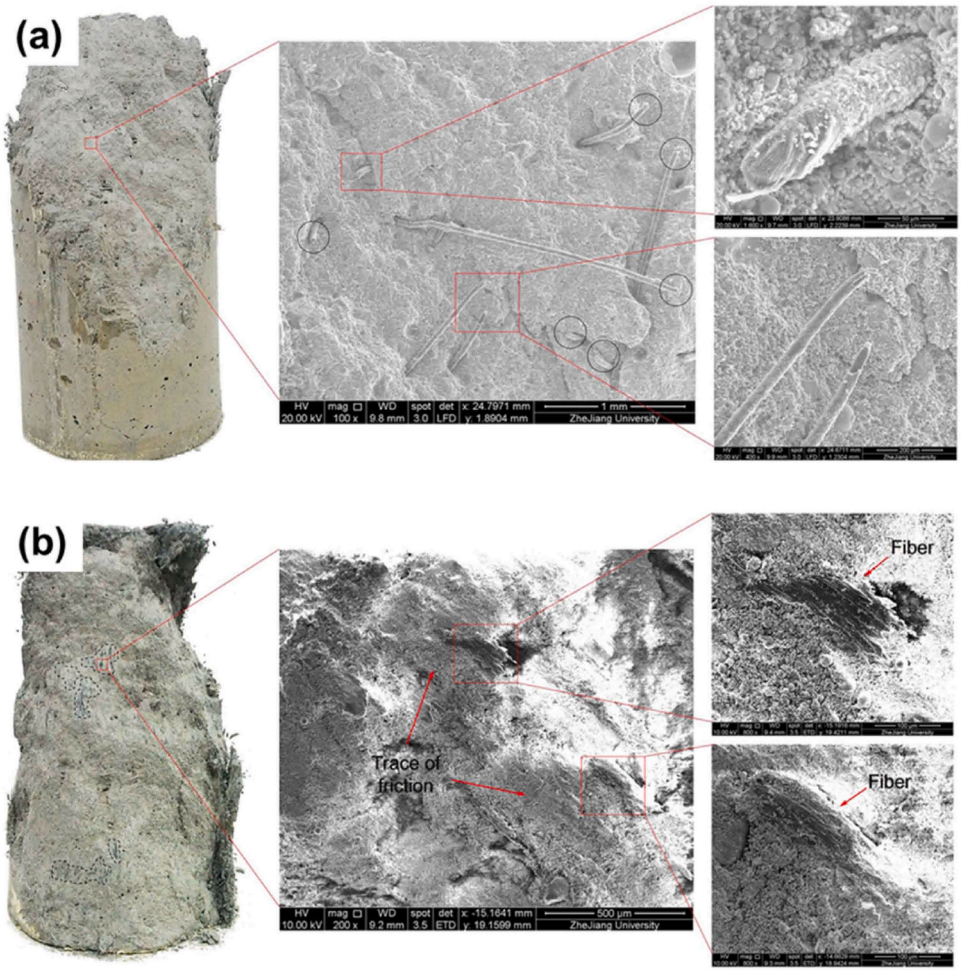

Fig. 12. Failure patterns of PVA fiber reinforced UHTCC under static and fatigue compression [77]: (a) Static compression; (b) Fatigue compression.

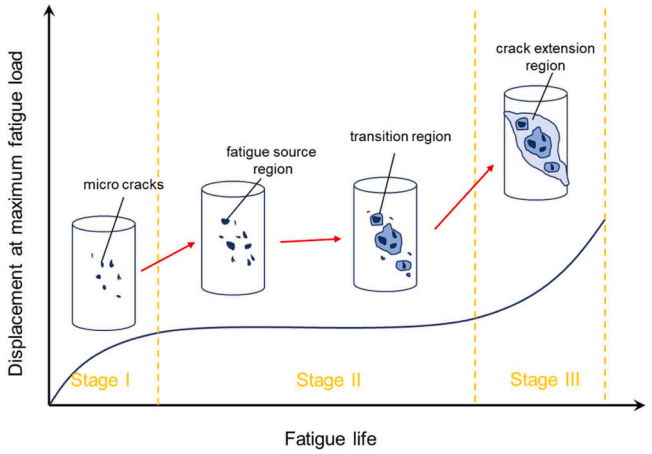

Fig. 13. The crack extension process of UHTCC under fatigue compression load [78].

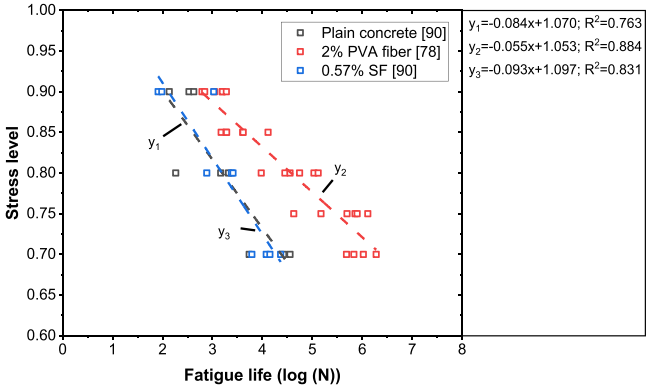

Fig. 14. Compression fatigue life of UHTCC under different stress level.

Fatigue life, the number of fatigue load cycles, is commonly used to assess the ability of concrete materials to resist fatigue loading. Fatigue test results are influenced by parameters such as loading frequency, level and direction [81–83]. Fig. 14 shows the fatigue life of plain concrete, 2 % PVA fiber reinforced UHTCC and 0.57 % SF reinforced concrete under different compression stress levels. A roughly linear relationship between fatigue life and stress level can be observed, with the fitting coefficients R^2 all exceeding 0.7. The concrete specimen with 0.57 % SF by volume is similar to plain concrete in a way that when the stress level increased from 0.70 to 0.90, both of their fatigue lives decreased from 10^4 to around 10^2. PVA fibers with a volume fraction of 2 % can effectively improve the fatigue life of cementitious composite at the same stress level. However, when the stress level increased from 0.70 to 0.90, the fatigue life of PVA fiber reinforced UHTCC decreased rapidly from 10^6 to 10^3.

The fatigue life of plain concrete and UHTCC does not show a strong linear relationship with the frequency of compressive loading, as shown

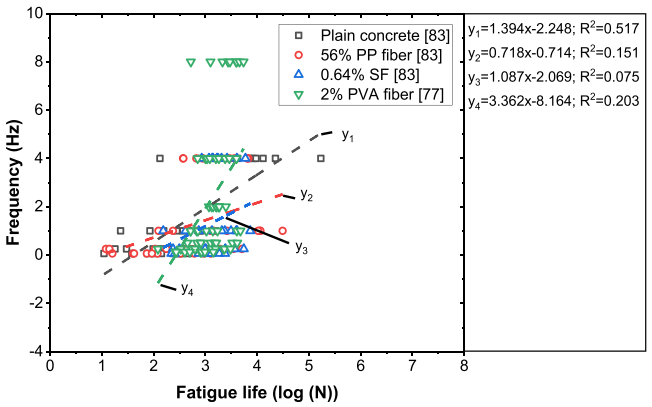

Fig. 15. Compression fatigue life of UHTCC under different frequency.

in Fig. 15. However, it can still be seen that the fatigue resistance of composite materials is more evident at higher loading frequencies. According to the test results of UHTCC under dynamic compression loading summarised in Section 3, a high strain rate enhances the ultimate strength before the failure of UHTCC [84]. As a result, UHTCC can withstand more loading cycles under a higher frequency cyclic loading. In addition, the difference in fatigue life of UHTCC with plain concrete and ordinary fiber reinforced concrete at various compression loading frequencies is not as significant as that under changing stress level conditions, which may be due to that the strain rate effect weakens the contribution of fibers [85–87].

More researchers tested the flexural fatigue life of UHTCC beams. The mechanical properties of concrete are strongly influenced by the mixture ratio, therefore, even for plain concrete, there are still significant differences in studies at the same stress level [88–90]. Similar to the results in Fig. 14 there is a clear linear relationship between flexural fatigue life and stress level for plain concrete and UHTCC in Fig. 16, except for y_4. PP fiber, PE fiber and PVA fiber can all bridge cracks and improve the flexural fatigue life of UHTCC especially at a higher stress level [91,92].

5. Dynamic performance of UHTCC under destructive penetration loads

5.1. Drop weight load

The restraining effect of fibers on cracks results in strong damage tolerance and high energy dissipation capacity of UHTCC specimens, which means that the UHTCC plate can maintain its integrity under large magnitude impact load [93]. Drop weight impact test is often used for the dynamic properties of concrete slabs subjected to multiple loads

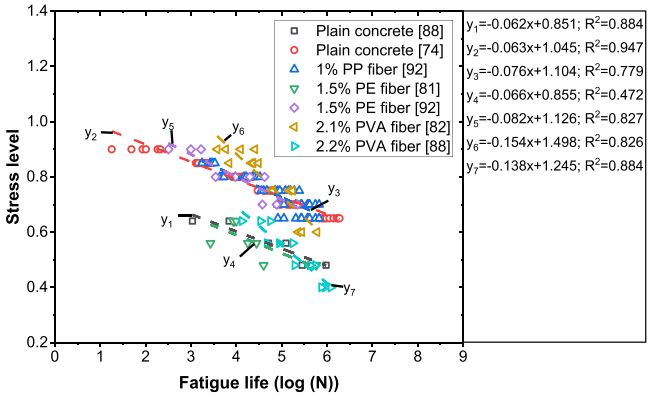

Fig. 16. Flexural fatigue life of UHTCC under different stress level.

with constant impact energy [94]. According to the applied impact energy and the crack development pattern, the dynamic performance of the UHTCC can be assessed.

The number of drop hammer blows corresponding to the appearance of the first crack and the final destruction of UHTCC specimens with different fibers were collected and shown in Fig. 17. Plain concrete cracked and damaged in the 8th drop weight loads, indicating that plain concrete presented little ductility without fiber reinforcement [95,96]. After the addition of PP fiber with a volume fraction of 1.5 % or PVA fiber with a volume fraction of 1 % to the composite, the number between first crack blow and failure blow appeared to be different, which signified that there was a certain degree of ductility in the composite materials at this time [97]. When the volume fraction of PVA fiber increased to 2 %, the ductility of the composite was significantly enhanced with the most significant difference resulting in Ismail et al.'s research [96,98]. The difference between the number of first crack blow and failure blow was more than 300. In addition, PE fiber with a volume fraction of 2 % also had a significant enhancement effect on the ductility of concrete [99]. In the study by Ismail et al., [96,98] the number of first crack blow of 2 % PVA fiber reinforced UHTCC was 69, whereas the number of failure blow increased to 351. Due to the high tensile strength and elastic modulus of SF, 2 % SF reinforced UHTCC presented the most excellent drop weight impact resistance [98]. The number of blows corresponding to the first crack of SF reinforced UHTCC was 200, and the number of final failure blow was up to 717. However, the hybrid fiber reinforced UHTCC consisting of 1 % PVA fiber and 1.5 % PP fiber did not exhibit the strain-hardening phenomenon that was so evident in the study of Ismail et al. [98,100]. This may be related to the design of the mixture proportion and the drop weight testing program (including the weight and height of the drop hammer) [101–103].

Fig. 18 shows the impact energy of UHTCC panels subjected to drop weight loads. The impact energy results are similar to the number of cracking blows, and the initial cracking energy of plain concrete is the same as that of failure impact energy, which was only 160 J. When concrete contains 1.5 % PP fiber or 1 % PVA fiber in concrete, the energy dissipation performance of concrete slabs during drop weight impact was significantly enhanced [97,103]. In the test results of Ismail et al. [96,98] the initial cracking impact energy of 2 % PVA fiber reinforced UHTCC reached about 1700 J and the failure impact energy reached about 8000 J, whereas this difference was not significant in the

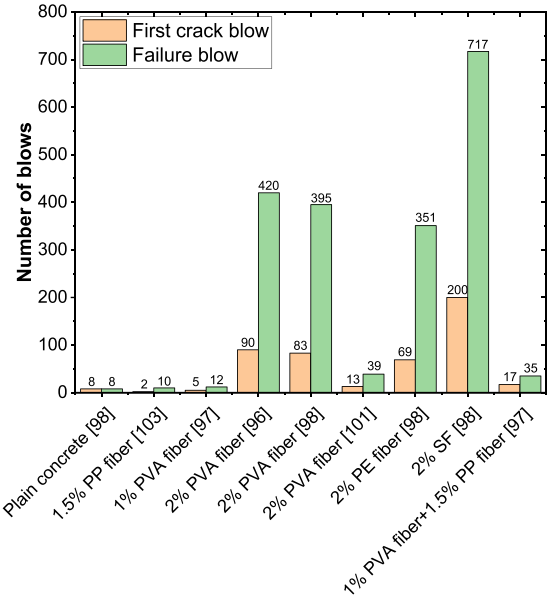

Fig. 17. The number of the first crack occurred and final failure blows of UHTCC specimens.

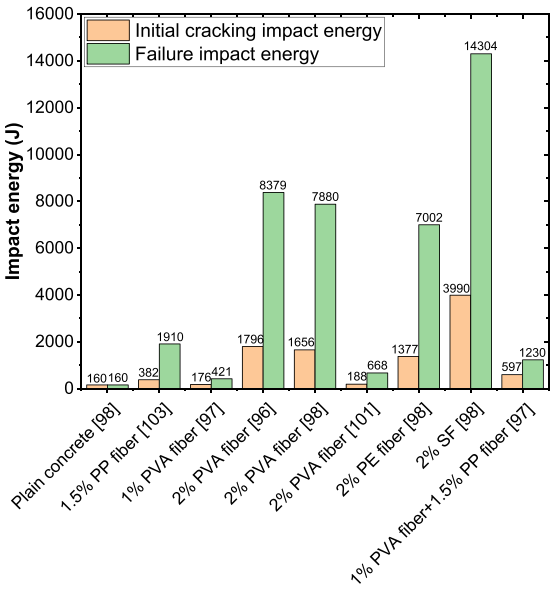

Fig. 18. The first cracking impact energy and final cracking impact energy of UHTCC specimens.

drop weight test results for the UHTCC with 1 % and 2 % PVA fiber by volume in Lin's and Ali's research, respectively [97,101]. This is mainly because of the difference in the physical properties of PVA fiber and the curing age of UHTCC specimens [97,101]. The contribution of PE fiber on the energy dissipation performance of UHTCC under drop weight impact was slightly lower than that of PVA fiber, but there was still a difference of 5625 J between the initial cracking impact energy and the failure impact energy [98]. The energy dissipation enhancement of SF on UHTCC specimens under drop hammer impact was the most obvious, with the initial cracking impact energy and failure impact energy reaching 3990 J and 14304 J, respectively [98]. In contrast to the number of blows, the composite materials containing 1 % PVA fiber and 1.5 % PP fiber exhibited a certain degree of energy dissipation capacity [94]. However, this was not as evident as that of composites reinforced with 2 % PVA, PE, and SF [94].

5.2. *High speed projectile impact*

For building with higher safety requirements, such as hydroelectric dams, nuclear power plants and military installations are generally required to withstand projectile impacts with higher strain rates [104]. Researchers used a smoothbore powder gun to launch ogival-nosed projectiles to impact concrete slabs of finite thickness, as shown in Fig. 19 [105]. The morphology features of the crater on the front face, the scab on the rear face and the striking velocity and residual velocity are the most important indices to assess the projectile impact resistance of concrete materials.

A high-speed camera can be used to capture the speed of a projectile when it penetrates a concrete slab as well as when it leaves the slab [106–108]. Xu et al. [107,108] fabricated PVA fiber and SF-reinforced concrete slabs with a volume fraction of 2 %, respectively. Taking two plates connected to an electron oscillograph as a reference, the high-speed camera showed that the velocity of the projectile decreased by 19.0 % (from 1003 m/s to 812 m/s) after penetrating plain concrete slabs [104]. Under the similar striking velocity, the value decreased by 23.0 % and 58.0 % after penetrating concrete slabs containing PVA fiber and SF respectively [107,108]. This indicates that PVA fiber and SF can effectively dissipate the impact energy of the projectile at high striking velocity. Peng et al. [105] fabricated concrete slabs with a thickness of 50 mm and SF volume fraction of 2 %. The test results show that for projectiles with striking velocity between 256–478 m/s, the residual speed was reduced by 11.1 %−31.6 % after perforation [105].

The equivalent diameters of crater and scab are important indicators for evaluating the extent of damage to concrete slabs by projectiles [109,110]. When the projectile contacts the concrete slab, the front surface is in a complicated tensile-compressive stress state and a crater generates; when the projectile penetrates and leaves the concrete slab, the tensile stress wave forms a scab on the rear surface [109,110]. The difference on the mechanism of these two damage modes results in a scabbing area that is generally larger than the cratering area [109,110]. It can be seen from Fig. 20 that compared to plain concrete slabs in the study of Xu et al. [108], when the projectile passes through the concrete slab containing PVA fiber with a volume fraction of 2 %, the equivalent cratering diameter decreased by 27.0 %−44.9 % and the equivalent scabbing diameter decreased by 27.0 %−40.5 %. In addition, Peng et al. [105] reported that SF can also constrain the matrix and significantly reduced the diameter of the crater and scab. It should be noted that in addition to striking velocity and fiber reinforcement, the size of crater and scab is also affected by the thickness of the concrete slab, the concrete mixture ratio and the morphology of the projectile [47,104,111]. Since the thickness of the UHTCC slabs used by Maalej et al. [47] was only 75 mm (vs. 360 mm in Xu et al.'s research [108]), the equivalent diameter of the crater remained on concrete slabs containing 0.5 % SF and 1.5 % PE fiber was larger than the equivalent diameter of crater left on plain concrete slab in Xu et al.'s projectile impact tests [108].

The penetration depth in the projectile impact test of concrete slab can be defined as the distance from the front surface to the nose of the projectile or the distance from the front surface to the initial point of the scab [112]. It can be seen from Fig. 21 that within the same striking velocity range, the impact energy absorption effect of synthetic fiber was not obviously reflected on the penetration depth, especially for the thinner thickness plates in the studies of Maalej et al. [47]. When the striking velocity was between 500–1000 m/s, the penetration depth

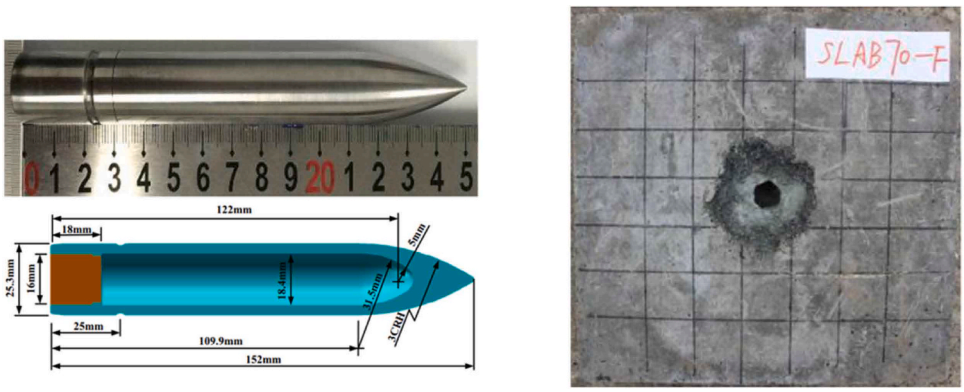

Fig. 19. The projectile and crater on a concrete slab after perforated test [105].

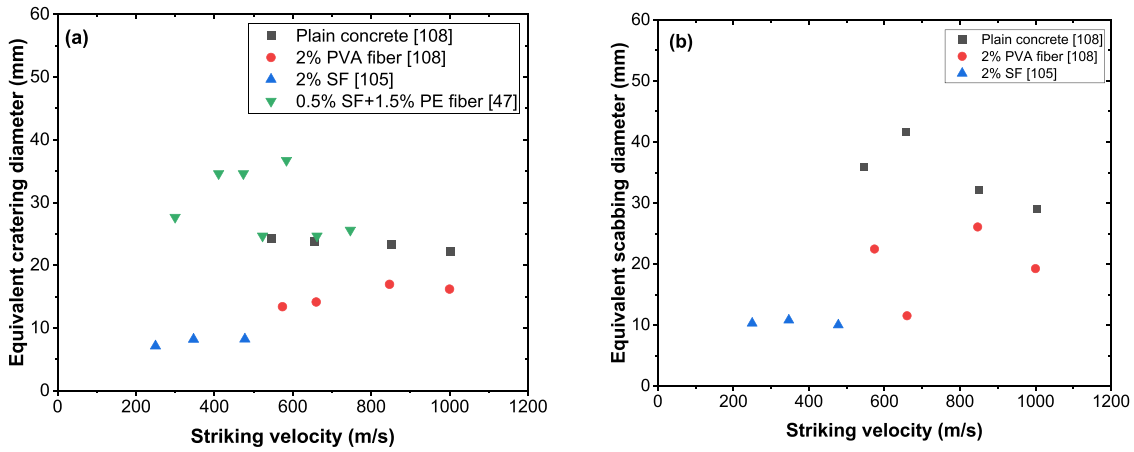

Fig. 20. Equivalent damage sizes of UHTCC slabs under projectile impact loads: (a) the equivalent cratering diameter; (b) the equivalent scabbing diameter.

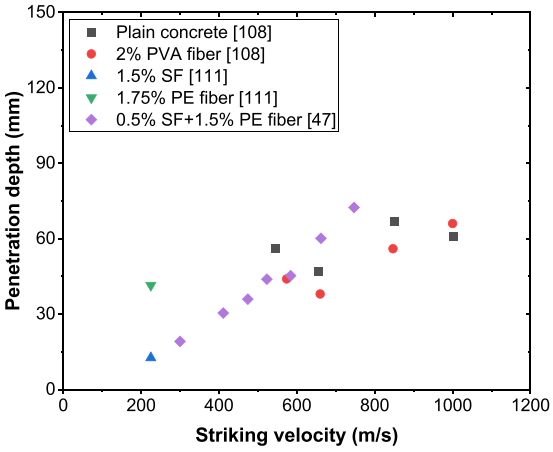

Fig. 21. The penetration depth of projectile impact tests on UHTCC slabs with different fibers.

remained between 40–70 mm for plain concrete and UHTCC slabs. This is because the fibers provide strain hardening behavior to the concrete slab and help dissipate fracture energy. As a result, concrete slabs reinforced with PVA fiber, PE fiber and SF maintained better integrity after projectile impact. The scabbing area of UHTCC slabs was smaller than plain concrete slabs, which avoids spalling and splashing of concrete fragments at the rear surface of the slabs as shown in Fig. 22. However, the projectile left a longer channel and therefore a larger penetration depth at this time. In addition, Xu et al. [108] observed the lateral crack distribution of a concrete slab subjected to the impact of a projectile with 30 mm in diameter, which is shown in Fig. 23. They found that a wide main crack emerged on the side surface of the plain concrete slab, whereas several narrow parallel cracks distributed on the side surface of the concrete slab containing 2 % SF [108]. This demonstrates that SF provides a certain degree of strain-hardening capacity to the concrete slab. There were no significant cracks on the sides of the concrete slab containing 2 % PVA fiber, indicating that the dissipation of tensile stress waves by PVA fiber was more significant [108].

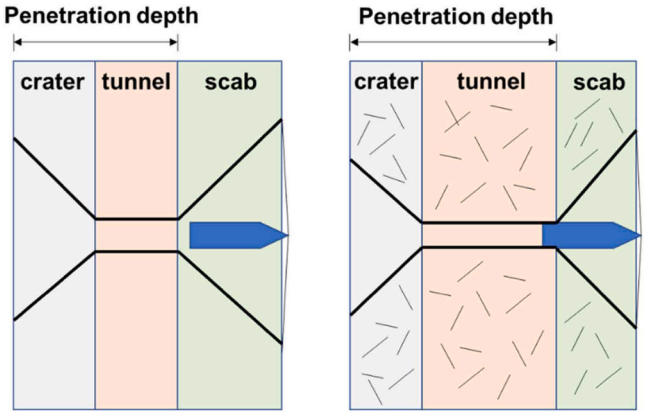

Fig. 22. Schematic diagram of projectile tests on plain concrete and UHTCC slabs.

5.3. Blast load

In today's unstable international situation, an increasing number of terrorist attacks or accidental explosions can expose concrete structures to impact loads with extremely high energy in an instant [107,109,113]. UHTCC materials with high energy dissipation capacity and fracture energy can effectively withstand explosion impact and prevent concrete debris from splashing and harming the public [112,114]. Similar to the damage caused by the projectile impact, blast loading would create a compressive stress wave and leave a crater on the front surface of the concrete slab [112,114,115]. The compressive stress wave conducted to

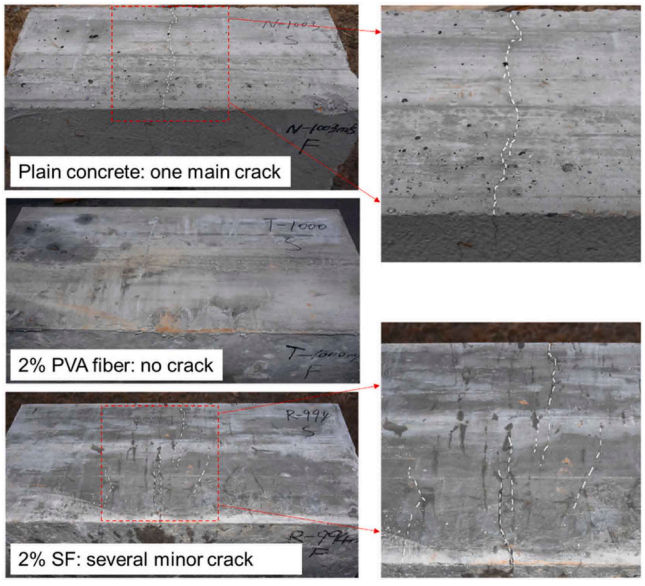

Fig. 23. The crack distribution of UHTCC slabs after suffering from projectile impact loads [108].

the back of the concrete slab transforms into a tensile-compressive stress interaction wave and forms a scab on the back surface [116,117]. Fig. 24 compared the damage of a normal RC slab and a UHTCC slab subjected to the same mass of TNT explosive impact. The size of the crater on the top surface of the concrete slab is larger than the size of the scab on the bottom surface. The UHTCC slab reinforced by fiber has smaller dimensions of damage from blast loads than normal reinforcement concrete (RC) for the same concrete matrix strength, reinforcement ratio, geometry size and amount of explosive used [118]. Xu et al. [119] conducted blast tests on concrete slabs and found that the crater created by 200 g TNT blast loads on ordinary RC slabs surrounded by numerous radial cracks and the concrete slab lost the ability to withstand loads. In contrast, there were fewer radial cracks on the front surface of the UHTCC slab, and the concrete fragments on the back surface were attached to the slab under the bonding effect of the PVA fiber on the cement matrix [119]. In the subsequent three-point bending tests, UHTCC slabs can still withstand bending loads of 40–70 kN after subjecting to blast impact [119]. Moreover, Chilvers et al. [118] collected and measured the concrete fragments produced by blast impacts on normal RC slabs and UHTCC slabs. The sizes of concrete fragments collected under normal RC slabs were distributed from blow 1.7 mm to above 19 mm, whereas the concrete fragments collected under UHTCC slabs were mainly above 19 mm [118]. This indicates that the bonding of fiber to the cement matrix played a key role in resisting the blast impact and reduced the splashing of small-sized concrete fragments.

Fig. 25 shows the damage diameter measured by researchers for normal RC panels and UHTCC panels. The test data in the different experiments varied considerably because the amount of TNT explosive, the geometry size and the heterogeneity of concrete panels had a large influence on the results [109,120,121]. Both 2 % PVA fiber, 2.5 % SF and hybrid fiber (1.75 % PVA fiber and 0.58 % SF) were effective in reducing the blast damage diameters of concrete panels. Specifically, crater damage diameter was reduced by 22.6 %, 50 % and 47.5 % respectively, whereas spall damage diameter was reduced by 66.8 %, 45.1 % and 34.4 % in these three groups of experiments. It is worth noting that the crater damage diameter on the top surface of the UHTCC panel with 2 % PVA fiber was larger than the spall damage diameter on the bottom surface because the UHTCC matrix fabricated by Li et al. [117] absorbed most of the blast impact energy, and the stress wave transmitted to the bottom surface was lower, which did not cause serious damage.

Note: In each group, the first two bars represent normal RC panels prepared in each experiment; the last two bars represent fiber-reinforced UHTCC panels.

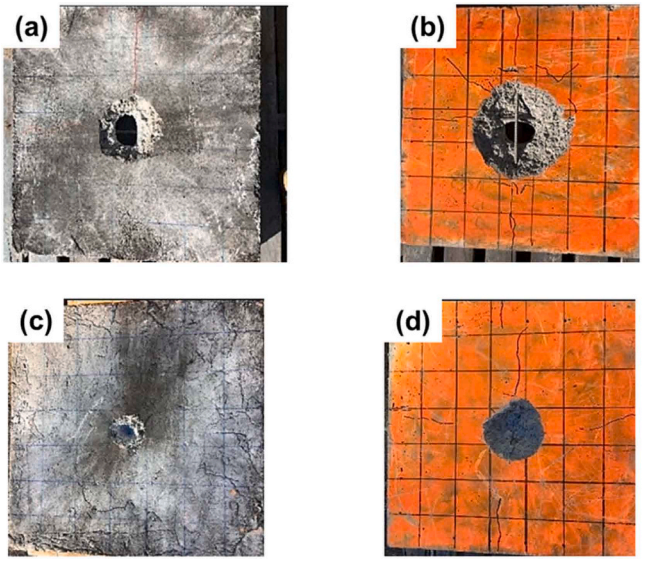

Fig. 24. Typical damage pattern of UHTCC panel after blast impact [118]: (a) Top surface of ordinary RC panel; (b) Bottom surface of ordinary RC panel; (c) Top surface of UHTCC panel; (d) Bottom surface of UHTCC panel.

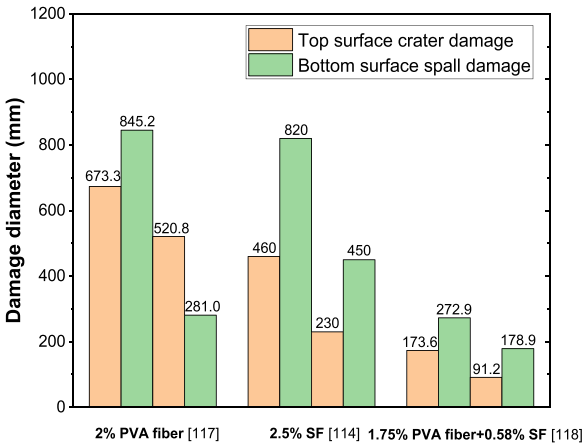

Fig. 25. Damaged diameter of UHTCC panels.

6. Seismic load for UHTCC structures and elements

The failure and collapse of concrete frame structures under seismic load are mainly induced by the insufficient shear strength and ductility of the plastic zones at beam-column joints [122–124]. For this reason, numerous researchers conducted seismic tests on reinforced concrete (RC) short columns to predict the performance of concrete frame structures under seismic load and to achieve better seismic resistance of concrete structures by taking advantage of the higher ductility and excellent energy dissipation properties of UHTCC [125–127].

The column-footing connection in the test contains a foundation beam and a short column, as shown in Fig. 26 (a). The loading devices include a hydraulic jack and a hydraulic actuator, which are used to apply constant axial loads and seismic loads, respectively. The column-footing connection is secured to the ground by steel plates and bolts. LVDTs and strain gauges are used to obtain hysteresis curves of the specimens under seismic loads.

Research usually use PVA fiber or PE fiber with volume fraction of 2 % to fabricate UHTCC reinforced concrete short columns [128,130]. Due to the restraining effect of PVA fiber and PE fiber on cracks, the RC short columns fabricated by UHTCC can still maintain their integrity after failure [127,128,130]. Bai et al. [128] reported that ordinary RC columns damaged by seismic loading formed a plastic hinge at 0–300 mm from the bottom, showing a bending-shear failure mode. However, the cracks from seismic loads on the short columns fabricated by UHTCC were dominated by fine and dense microcracks with plastic hinges rising up to 250–500 mm from the bottom [128]. Fig. 26 (b) shows the skeleton of hysteresis curves obtained in seismic tests. Based on these curves, PVA fiber and PE fiber with a volume fraction of 2 % can enhance the peak load and ultimate load of RC columns in seismic tests, while a more significant improvement was observed in the deformation capacity. Bai et al. [128] found that the UHTCC reinforced concrete columns had an enhancement of 4.3 % in ultimate load over normal reinforced concrete columns, whereas the enhancement in ultimate displacement was 23.8 %. Zhang et al. [125] showed that the peak load of UHTCC-reinforced concrete columns containing 2 % PVA fiber was elevated by 22.9 %, while the peak displacement was improved by 49.6 % compared to normal RC columns. Similarly, Wu et al. [129] reported that the peak load of UHTCC-reinforced concrete columns decreased by 14.2 % compared to normal RC columns, while the peak displacement was enhanced by 8.5 %. The decrease in seismic load capacity of UHTCC columns is mainly due to the difference in the mixture ratio of concrete [129,131,132]. In Wu et al.'s experiments [129], the cubic compressive strength of plain concrete was 69.2 MPa, whereas the

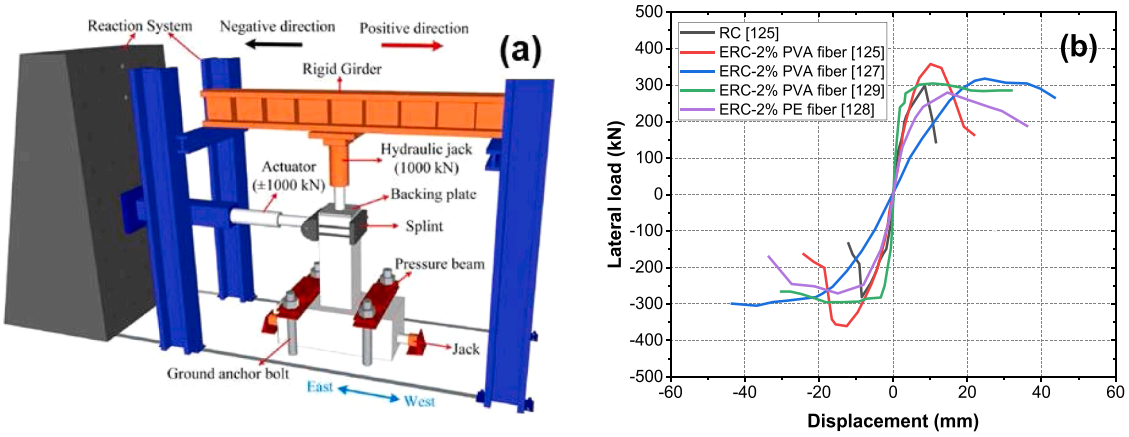

Fig. 26. Seismic tests for UHTCC columns: (a) Seismic test setup for UHTCC column [128]; (b) Skeleton of hysteresis curves [125,127–129].

cubic compressive strength of UHTCC was only 49.7 MPa.

In comparison to yield point, peak point and ultimate point of hysteresis curves, the conclusion of existing studies on cumulate energy (E_c), displacement ductility coefficient (μ) and ultimate drift ratio (θ_u) are more consistent [125,126,129,133]. Table 1 summarizes the results of existing seismic experiments on UHTCC-reinforced concrete columns. Interfered by mixture ratio, fiber distribution, loading scheme and spalling of debris, fibers may present a negative effect on the displacements and forces at critical points of seismic hysteresis curves in the test results of some researchers [123,125,131]. In contrast, E_c, μ and θ_u, which are calculated by geometrical size, deformation and seismic loads applied to the UHTCC columns, can provide a more stable assessment of the contribution of fibers in seismic tests. As shown in Table 1, the available test results all indicate that fibers improve the plastic deformation performance and energy dissipation performance of concrete columns under seismic loads. Specifically, the test data of Zhang et al. [125] show that the μ and θ_u of UHTCC-reinforced concrete columns with a volume fraction of 2 % PVA fiber were improved by 42.0 % and 77.4 %, respectively, compared to those of ordinary RC. Yuan et al. [126] found that E_c of UHTCC reinforced concrete columns at the ultimate state was 72.5 % higher than that of ordinary RC columns.

In addition to column-footing connections, Qudah and Maalej [135] tested the seismic behavior of UHTCC beam-column connections. The results show that replacing the plain concrete in the plastic joints of beam-column connection with UHTCC can effectively improve the seismic energy absorption capacity, shear force resistance and cracking performance of joints [135]. Similarly, Abbas et al. [131] found that 1.5 % SF improved the energy absorption performance of beam-column connections by 3.8 times and ductility ratio by 1.5 times. For more complicated structures, Yu et al.'s [136] focus was directed towards examining the impact of reinforcing masonry walls with ECC layers. The experimental findings unveiled significant alterations in various response parameters, including acceleration, strain, displacement, and dynamic characteristics both before and after the application of ECC strengthening [136]. Overall, the outcomes underscored a substantial enhancement in the impact resistance of masonry walls subsequent to ECC layer reinforcement [136]. Furthermore, it was observed that the presence of the ECC layer had the advantageous effect of shifting the failure mode from brittle to a more ductile behavior, even when subjected to higher levels of impact [137]. Deng et al. [138] and Dong et al. [130] established two-story masonry buildings using PVA fiber reinforced UHTCC as shown in Fig. 27. They applied seismic loads on two-story structures by a shaking table and found that UHTCC significantly increased the shear capacity and overall stiffness of damaged masonry [130,138]. No noticeable main cracks or detachments were observed on the UHTCC overlay [130,138]. Walls retrofitted with UHTCC overlays exhibited robust resistance to seismic loads and maintained adequate safety margins under 9 R degree (peak ground acceleration = 1.171 g) earthquakes in comparison to traditional masonry and confined masonry wall structures [130,138].

7. Numerical simulation of UHTCC specimens and structures under dynamic loads

Dynamic experiments usually have a low effective-cost ratio, especially for projectile impact tests, blast tests and seismic tests, and researchers often only obtain failure patterns as test results, which prompts the use of numerical simulations [134–136]. Table 2 summarizes the existing numerical simulation methods for the dynamic performance investigation on UHTCC. Among them, ABAQUS and

Table 1
Summary of seismic test results of UHTCC columns.

Fiber type	λ	P_a (kN)	Yield point		Peak point		Ultimate point		E_c	μ	θ_u	Refs.
			D_y	P_y	D_p	P_p	D_u	P_u				
2 % PVA fiber	1.5, 2	515.6	↑	↑	↑	↑	↑	↑	↑	↑	↑	[125]
2 % PVA fiber	3.25	1222	-	-	↓	↓	↑	↓	↑	—	—	[127]
2 % PVA fiber	2	350	↓	↓	↑	↓	-	—	—	↑	↑	[129]
2 % PVA fiber	1.6	224 −1242	~	↑	~	↑	↑	↑	↑	↑	-	[126]
2 % PE fiber	2.5	596	↑	↑	↑	↑	↑	↑	-	↑	↑	[128]
2 % SF	4.2	550.5 −1406	↓	↑	↑	↑	↑	↑	↑	↑	↑	[134]
1.5 % SF	4	1000	~	~	~	~	↑	—	↑	—	—	[133]
0.15 % PP fiber	4	1000	↑	↑	↑	↑	↑	—	↑	—	—	[133]
1.5 % SF+ 0.15 % PP fiber	4	1000	↑	↑	↑	↑	↑	—	↑	—	—	[133]

Note: λ represents shear span-to-depth ratio; P_a represents axial load; D_y and P_y represents yield displacement and yield load respectively; D_p and P_p represents peak displacement and peak load respectively; D_u and P_u represents ultimate displacement and ultimate load respectively; E_c represents ultimate cumulate energy; μ represents displacement ductility coefficient; θ_u represents ultimate drift ratio; symbol '↑' represents positive effect; symbol '↓' represents negative effect; symbol '~' represents no clear effect; symbol '—' represents the parameter was not analysed in the study.

Fig. 27. The two-story masonry building with UHTCC layer and crack patterns under seismic loads [138].

Table 2
Summarization of numerical simulation for UHTCC under dynamic loads.

Fiber type	Loading condition	Software	UHTCC model	Refs.
1 % and 2 % SF	Cyclic load	ABAQUS	Plastic-Damage model	[61]
2 % PVA fiber and 2 % nylon fiber	Drop weight load	ABAQUS	Concrete plastic-Damage model	[95]
—	Drop weight load, explosion, high-speed penetration	LS-DYNA	Improved Karagozian and Case concrete/ cementitious model	[112]
—	Blast and high-speed impact loading	LS-DYNA	Improved Holmquist-Johnson-Cook model	[107]
2 % PVA fiber	High-speed impact and contact blast loads	LS-DYNA	A dynamic constitutive model	[109]
0.5 % SF, 1.5 % PE fiber and 2 % PVA fiber	High-velocity projectile impact	LS-DYNA	Mat 72R3-Concrete Damage model	[106]
2 % PVA fiber	Blast load	LS-DYNA	Concrete Damage Model (MAT72 R3)	[119]
2 % PE fiber and 2 % SF	Blast load	LS-DYNA	Plasticity compression tension model (MAT124)	[113]
2 % PVA fiber	Contact explosion	LS-DYNA	improved Karagozian & Case model (MAT72R3)	[117]
1.75 % PVA fiber and 0.58 % SF	Contact explosion	LS-DYNA	improved Karagozian & Case Concrete model	[118]
1 %, 1.5 %, 2 % and 2.5 % SF	Seismic load	ABAQUS	Brittle cracking model	[131]
2 % PE fiber	Seismic load	ABAQUS	Concrete damage plastic model	[128]

LS-DYNA are the most used finite element modelling software. Yildirim et al. [95] used three-dimensional 10-node modified tetrahedrons (C3D10M) in ABAQUS software to develop a finite element model of a UHTCC beam. They found that the concrete damage plasticity model, which is commonly used to represent the inelastic behavior of concrete cannot accurately reflect the unique strain-hardening capability of UHTCC materials subjected to sudden impact loads [95]. Yin et al. [112] reported that the explicit simulation software LS-DYNA and Karagozian & Case concrete/cementitious model (K & C model) can accurately simulate the explosion and projectile penetration damage of concrete slabs, whereas the simulation of seismic load and low-velocity impact was less accurate. Considering the bridge effect of fibers on cracks, Yin et al. [112] systematically modified the K & C model parameters for UHTCC. The accuracy of the calibrated parameters was verified using data from drop weight tests, projectile penetration tests and explosion tests [112]. Wu et al. [109] developed a dynamic constitutive model considering the damage evolution and strain-hardening properties of UHTCC. The LS-DYNA software was used to simulate the projectile penetration and blast loads of the UHTCC panel [109]. Compared with the traditional Holmquist-Johnson-Cook (HJC) model, Riedel-Hiermaier-Thoma (RHT) model and K & C model, the dynamic model proposed by Wu et al. [109] has minimal error in predicting damage sizes of UHTCC panels subjected to projectile penetration and blast loads. Liao et al. [113] pointed out that the stress-strain curve of UHTCC under directed tension has an obvious plateau stage, while ordinary concrete is a typical brittle material. The numerical models that have been widely used to analyze concrete materials, such as the K & C model and HJC model, may not be suitable for analyzing the dynamic performance of UHTCC under blast loads [113]. Therefore, Liao et al. [113] selected a plasticity compression tension model (MAT 124), which is commonly used to describe metals and plastics in the LS-DYNA software, to describe the behavior of UHTCC at high strain rates. The numerical analysis results show that UHTCC with high scale distance and reinforcement ratio possesses better explosive resistance capacity [113]. Xu et al. [107,119] proposed an explicit dynamic constitutive model suitable for analyzing the dynamic performance of UHTCC by improving HJC model. Compared with experimental data, the model proposed by Xu et al. [107,119] can predict the damage caused by embedded explosion and projectile impact loads on UHTCC panels (with the error of crater size, penetration depth and crack distribution lower than 5 %). For the numerical simulation of the seismic performance of concrete structures, Abbas et al. [131] created a 3D nonlinear finite element model using ABAQUS software. The parametric analysis results show that a reasonable SF content (volume fraction of around 1.5 %) can restrain crack extension under seismic loads and significantly improve the ductility of concrete structures [131]. Bai et al. [128] used concrete damage plastic model in ABAQUS to analyze the seismic performance of a concrete column. As shown in Fig. 28, the plastic hinge of the normal RC column under seismic loading appeared at the column-foundation connection. The plastic hinge can be relocated away from the column-footing connection by using UHTCC and pre-embedded H-shaped steel. Compared to the normal H-shaped steel reinforced column, the RC column fabricated by UHTCC can spread seismic loads to a larger area, which enhances the plastic deformation ability of the column [139–142].

8. Conclusions and perspectives

This paper presents a review of the research progress of fiber-reinforced UHTCC under various dynamic loads. The influences of fiber type and strain rate on the strain-hardening behavior, high ductility and energy dissipation ability of UHTCC were the focus of attention. The roles played by fibers under various loading conditions were analyzed from theoretical aspects. Finally, the applicability of UHTCC on concrete structures has been confirmed by shaking table tests

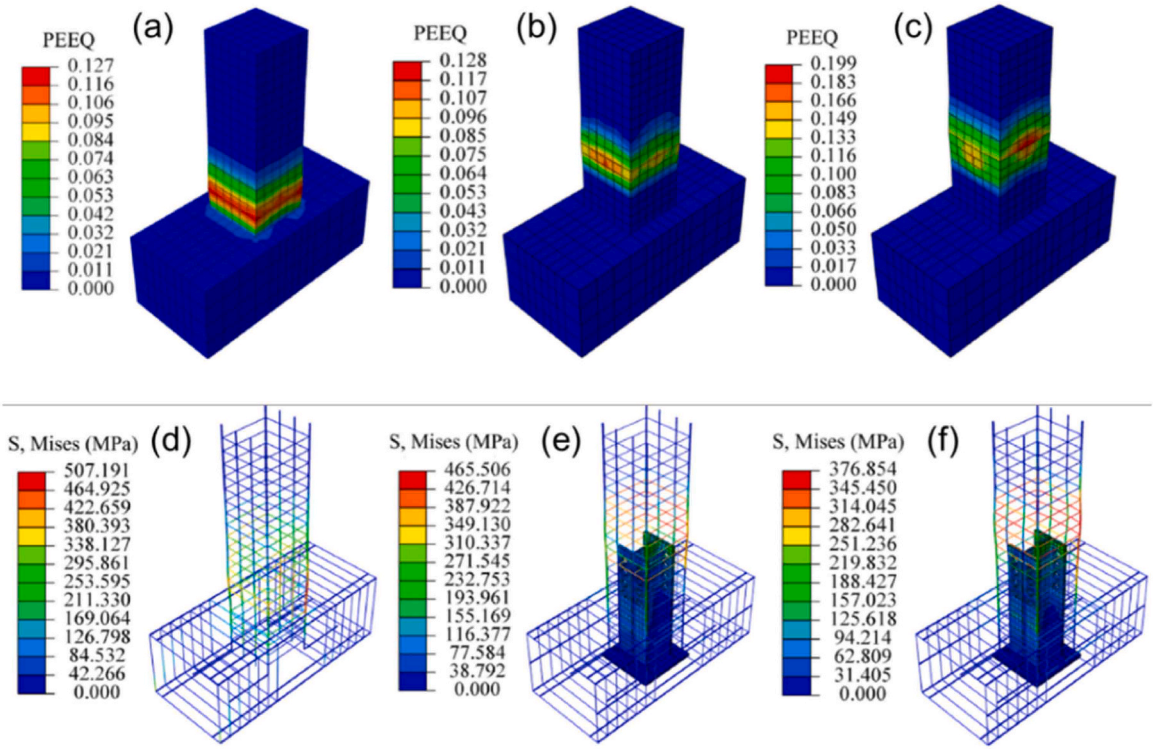

Fig. 28. Finite element analysis of normal RC and UHTCC columns [128]: (a) Equivalent plastic strain of normal RC column; (b) Equivalent plastic strain of H-shaped steel RC column; (c) Equivalent plastic strain of UHTCC column; (d) Steel skeleton of normal RC column; (e) Steel skeleton of H-shaped steel RC column; (f) Steel skeleton of UHTCC column.

and finite element simulations. Based on the stress-strain curves and damage patterns obtained in the existing research, the following conclusions can be drawn up:

(1) Synthetic fiber can restrain the crack extension of cementitious composite under dynamic loads and enhance the energy dissipation capacity of the material. The peak strain and post-peak ductility of the dynamic compressive stress-strain curve of UHTCC were higher than those of plain concrete. The combined use of SF and synthetic fiber such as PE fiber and PVA fiber can effectively improve the dynamic compressive strength and dynamic tensile strength without obviously sacrificing the strain-hardening ability of UHTCC.

(2) The dynamic compressive strength, dynamic compressive energy dissipation and dynamic tensile strength of UHTCC gradually increased with strain rate and the peak stress of UHTCC was more sensitive to strain rate than plain concrete according to DIF. The deformation ability of UHTCC decreased with the increase of tensile strain rate. When the tensile strain rate exceeded 30 s^{-1}, the UHTCC may lose the strain-hardening ability and exhibit brittle damage characteristics, because the fracture damage of fiber predominated at a high strain rate.

(3) The flexural strength of UHTCC beams subjected to dynamic bending loads increased gradually with strain rate, whereas the ductility decreased steadily, which was caused by fiber breakage at a high strain rate. UHTCC beams with SF can withstand bending loads with higher strain rates and maintain their integrity after damage.

(4) SF and PP fiber with high tensile strength can restrain crack expansion and elevate peak stress of UHTCC specimens under cyclic compressive loads and bending loads. In comparison, the peak stress of UHTCC specimens under cyclic tensile loads was less affected by SF because the tensile load is more sensitive to microcracks, and the excess SF increased the volume fraction of the weak zone within the matrix.

(5) The compression fatigue life and flexural fatigue life of UHTCC showed a strong linear relationship with stress level. PP fiber, PVA fiber, PE fiber and SF can enhance the fatigue life of UHTCC. However, the linear relationship between compression fatigue life and compression frequency was not obvious, and the fatigue life of UHTCC under high-frequency fatigue compression loads was not significantly different from that of plain concrete. This is probably because high strain rate weakens the reinforcement effect of fiber.

(6) The energy dissipation performance of UHTCC slabs under drop weight load, projectile impact load and blast load was higher than that of plain concrete. UHTCC panels containing 2 % PE fiber, PVA fiber and SF by volume can withstand more impact loads. Moreover, projectile impact load and blast load caused less damage size to UHTCC slabs than normal concrete because of the restraining effect of fibers on matrix.

(7) RC structures with UHTCC as matrix had higher ductility, plastic deformation capacity and energy dissipation ability under seismic loads. The application of UHTCC in the column-footing connection helped relocate the plastic hinge to the middle of the column from the root and spread seismic loads to a larger area. For masonry buildings, UHTCC overlay with PVA fiber can improve shear capacity and ductile behaviour.

(8) Researchers usually choose ABAQUS and LS-DYNA software for numerical simulation of UHTCC structures. Conventional models for ordinary concrete materials cannot reflect the strain-hardening characteristics of UHTCC, especially when the specimens are subjected to seismic loads and low-velocity impact loads. For finite element analysis of UHTCC structures under dynamic loads, it is necessary to adjust the existing model to enhance the importance of plastic deformation parameters.

(9) UHTCC is produced through a systematic design of cementitious matrix and fiber based on the fracture mechanics and micro-mechanics. It achieves a tensile capacity of more than 3 % and the higher tensile strength than plain concrete. High bonding strength at fiber-matrix interface would negatively impact the deformation ability of UHTCC, whereas the low bonding strength at fiber-matrix interface would reduce the ultimate strength under dynamic loads. A clearer connection needs to be established between the fiber-matrix interface bonding strength and dynamic performance of UHTCC.

(10) Due to the satisfying tensile strength, plastic deformation ability and energy dissipation capacity, UHTCC has the potential to be used in building structures and improve their impact resistance. Currently popular smart construction technologies, such as 3D printing, can be attempted to produce UHTCC elements, and the dynamic properties of 3D printed UHTCC specimens deserve investigation.

(11) The fibers commonly used to prepare UHTCC are synthetic fibers and SF, which cause energy consumption and environmental pollution. The deformation performance and energy consumption capacity of UHTCC with low-carbon and sustainable fibers and related modified fibers require further examination.

CRediT authorship contribution statement

Liangming Sun: Writing – review & editing, Writing – original draft, Visualization, Supervision, Resources, Conceptualization. **Wengui Li:** Writing – review & editing, Writing – original draft, Supervision, Resources, Conceptualization. **Shuguang Liu:** Writing – review & editing, Writing – original draft, Investigation, Funding acquisition, Formal analysis. **Hanbing Zhao:** Writing – review & editing, Writing – original draft, Validation, Investigation, Conceptualization. **Umar Muhammad:** Writing – review & editing, Writing – original draft. **Da Chen:** Writing – review & editing, Writing – original draft.

Declaration of Competing Interest

The authors declare that they have no known competing financial interests or personal relationships that could have appeared to influence the work reported in this paper.

Data Availability

Data will be made available on request.

Acknowledgements

The authors would like to acknowledge the support from Australian Research Council (ARC), Australia (FT220100177, LP230100288, DP220101051, DP220100036, IH200100010), National Natural Science Foundation of China (51608410), Hubei Key Laboratory of Roadway Bridge and Structure Engineering (Wuhan University of Technology) (DQJJ201905), and Wuhan Municipal Urban-Rural Development Bureau Science and Technology Plan Project (202205, 202304).

References

[1] Yu Q, Zhuang W, Shi C. Research progress on the dynamic compressive properties of ultra-high performance concrete under high strain rates. Cem Concr Compos 2021;124:104258.
[2] Das N, Nanthagopalan P. State-of-the-art review on ultra high performance concrete - Ballistic and blast perspective. Cem Concr Compos 2022;127:104383.
[3] Esaker M, Thermou GE, Neves L. Impact resistance of concrete and fibre-reinforced concrete: A review. Int J Impact Eng 2023;180:104722.
[4] Ozbolt J, Sharma A, Reinhardt H-W. Dynamic fracture of concrete-compact tension specimen. Int J Solids Struct 2011;48:1534–43.
[5] Tang Z, Li W, Tam VWY, Luo Z. Investigation on dynamic mechanical properties of fly ash/slag-based geopolymeric recycled aggregate concrete. Compos B Eng 2020;185:107776.
[6] Zhang B, Feng Y, Xie J, He J, Zhang Y, Cai C, Huang D, Li L. Effects of fibres on ultra-lightweight high strength concrete: Dynamic behaviour and microstructures. Cem Concr Compos 2022;128:104417.
[7] Hao Y, Hao H, Jiang GP, Zhou Y. Experimental confirmation of some factors influencing dynamic concrete compressive strengths in high-speed impact tests. Cem Concr Res 2013;52:63–70.
[8] Zhu J, Xu L, Huang B, Weng K, Dai J. Recent developments in engineered/strain-hardening cementitious composites (ECC/SHCC) with high and ultra-high strength. Constr Build Mater 2022;342:127956.
[9] Yoo D-Y, Banthia N. High-performance strain-hardening cementitious composites with tensile strain capacity exceeding 4%: a review. Cem Concr Compos 2022;125:104325.
[10] Singh M, Saini B, Chalak HD. Performance and composition analysis of engineered cementitious composite (ECC.) – A Rev, J Build Eng 2019;26:100851.
[11] Shanmugasundaram N, Praveenkumar S. Influence of supplementary cementitious materials, curing conditions and mixing ratios on fresh and mechanical properties of engineered cementitious composites – a review. Constr Build Mater 2021;309:125038.
[12] Ahmed SFU, Mihashi H. A review on durability properties of strain hardening fibre reinforced cementitious composites (SHFRCC). Cem Concr Compos 2007;29:365–76.
[13] Du W, Yang C, Wang C, Pan Y, Zhang H, Yuan W. Flexural behavior of polyvinyl alcohol fiber–reinforced ferrocement cementitious composite. J Mater Civ Eng 2021;33(4):04021040.
[14] Shi Y, Shi ZM. Surface treatment of cementitious composites by ultrasound and its effect on durability performance. J Mater Civ Eng 2021;33(3):04020487.
[15] Ali MAEM, Nehdi ML. Innovative crack-healing hybrid fiber reinforced engineered cementitious composite. Constr Build Mater 2017;150:689–702.
[16] Wishwesh KV, Anand KB. PVA Fiber-fly ash cementitious composite: assessment of mechanical properties. Inter J Civ Eng Tech (IJCIET) 2017;8(10):647–58.
[17] Lei D, Guo L, Chen B, Curosu I, Mechtcherine V. The connection between microscopic and macroscopic properties of ultrahigh strength and ultra-high ductility cementitious composites (UHSUHDCC). Compos B Eng 2019;164:144–57.
[18] Huang B, Zhu J, Weng K, Li VC, Dai J. Ultra-high-strength engineered/strain-hardening cementitious composites (ECC/SHCC): Material design and effect of fiber hybridization. Cem Concr Compos 2022;129:104464.
[19] Lao J, Ma R, Xu L, Li Y, Shen Y, Yao J, Wang Y, Xie T, Huang B. Fly ash-dominated high-strength engineered/strain-hardening geopolymer composites (HS-EGC/SHGC): influence of alkalinity and environmental assessment. J Clean, Prod 2024;447:141182.
[20] Wang Z, Liu Y, Shen RF. Stress–strain relationship of steel fiber-reinforced concrete under dynamic compression. Constr Build Mater 2008;22:811–9.
[21] Guo A, Zhou F, Du Y, Yan R. Dynamic Compressive Behavior of CTRC and ECC Layered Concrete under Impact Load. KSCE J Civ Eng 2021;25(11):4374–85.
[22] Kai MF, Xiao Y, Shuai XL, Ye G. Compressive behavior of engineered cementitious composites under high strain-rate loading. J Mater Civ Eng 2017;29(4):04016254.
[23] Zhao X, Li H, Wang C. Quasi-static and dynamic compressive behavior of ultra-high toughness cementitious composites in dry and wet conditions. Constr Build Mater 2019;227:117008.
[24] Chen Z, Yang Y, Yao Y. Effect of nanoparticles on quasi-static and dynamic mechanical properties of strain hardening cementitious composite. Adv Mech Eng 2019;11(5):1–11.
[25] Zhao J, Yang X, Fan J, Gao S, Ma H. Research on Dynamic Compressive Performance of Polypropylene Fiber-Reinforced High-Strength Concrete under Freeze-Thaw Environment. Adv Mater Sci Eng 2022.
[26] Guo L, Guo R, Yan Y, Zhang Y, Wang Z, Mu Y. Dynamic Compression Mechanical Properties of Polyoxymethylene-Fiber-Reinforced Concrete. Materials 2022;15:7784.
[27] Chen M, Wang Y, Zhang T, Zhang M. Microstructural evolution and dynamic compressive properties of engineered cementitious composites at elevated temperatures. J Build Eng 2023;71:106519.
[28] Zhang N, Zhou J, Ma G. Dynamic properties of strain-hardening cementitious composite reinforced with basalt and steel fibers. Int J Concr Struct Mater 2020;14(44).
[29] Li Q, Zhao X, Xu S, Leung CKY, Wang B. Multiple impact resistance of hybrid fiber ultrahigh toughness cementitious composites with different degrees of initial damage. J Mater Civ Eng 2019;31(2):04018368.
[30] Li Q, Zhao X, Xu S, Gao X. Influence of steel fiber on dynamic compressive behavior of hybrid fiber ultra high toughness cementitious composites at different strain rates. Constr Build Mater 2016;125:490–500.
[31] Zhang H, Wang L, Zheng K, Jibrin BT, Totakhil PG. Research on compressive impact dynamic behavior and constitutive model of polypropylene fiber reinforced concrete. Constr Build Mater 2018;187:584–95.
[32] Zhang N, Xu M, Song S, Li H, Zhou J, Ma G. Impact resistance of basalt fiber strain-hardening cementitious composites exposed to elevated temperatures. Constr Build Mater 2020;262:120081.
[33] Zhao X, Xu S, Li Q, Chen B. Coupled effects of high temperature and strain rate on compressive properties of hybrid fiber UHTCC. Mater Struct 2019;92.
[34] Hou X, Cao S, Zheng W, Rong Q, Li G. Experimental study on dynamic compressive properties of fiber-reinforced reactive powder concrete at high strain rates. Eng Struct 2018;169:119–30.

[35] Boshoff WP, Zijl GPAGv. Time-dependent response of ECC: characterisation of creep and rate dependence. Cem Concr Res 2007;37:725–34.
[36] Douglas KS, Billington SL. Strain rate dependence of HPFRCC cylinders in monotonic tension. Mater Struct 2011;44:391–404.
[37] Huo Y, Liu T, Lu D, Han X, Sun H, Huang J, Ye X, Zhang C, Chen Z, Yang Y. Dynamic tensile properties of steel fiber reinforced polyethylene fiber-engineered/strain-hardening cementitious composites (PE-ECC/ SHCC) at high strain rate. Cem Concr Compos 2023;143:105234.
[38] Li H, Xu S. Rate dependence of ultra high toughness cementitious composite under direct tension. J Zhejiang Univ-Sci A 2016;17(6):417–26.
[39] Li Q, Jiang X, Zeng T, Xu S. Experimental investigation on strain rate effect of high-performance fiber reinforced cementitious composites subject to dynamic direct tensile loading. Cem Concr Res 2022;157:106825.
[40] Li L, Wang H, Wu J, Li S, Wu W. Experimental investigation on dynamic tensile behaviors of engineered cementitious composites reinforced with steel grid and fibers. Materials 2021;14:7042.
[41] Zhao X, Yu X, Cai L, Peng Q, Wu H, Zhou F. The effects of tensile strain rate on the dynamic tensile behavior of ultra high toughness cementitious composite. J Build Eng 2023;68:106199.
[42] Ranade R, Li VC, Heard WF. Tensile rate effects in high strength-high ductility concrete. Cem Concr Res 2015;68:94–104.
[43] Yu K, Dai J, Lu Z, Poon CS. Rate-dependent tensile properties of ultra-high performance engineered cementitious composites (UHP-ECC). Cem Concr Compos 2018;93:218–34.
[44] Yang E-H, Li VC. Strain-rate effects on the tensile behavior of strain-hardening cementitious composites. Constr Build Mater 2014;52:96–104.
[45] Lu D, Wang G, Du X, Wang Y. A nonlinear dynamic uniaxial strength criterion that considers the ultimate dynamic strength of concrete. Int J Impact Eng 2017;103:124–37.
[46] Yan D, Lin G. Dynamic properties of concrete in direct tension. Cem Concr Res 2006;36:1371–8.
[47] Maalej M, Quek ST, Zhang J. Behavior of hybrid-fiber engineered cementitious composites subjected to dynamic tensile loading and projectile impact. J Mater Civ Eng 2005;17(2):143–52.
[48] Mechtcherine V, Silva FdA, Müller S, Jun P, Filho RDT. Coupled strain rate and temperature effects on the tensile behavior of strain-hardening cement-based composites (SHCC) with PVA fibers. Cem Concr Res 2012;42:1417–27.
[49] Mechtcherine V, Silva FdA, Butler M, Zhu D, Mobasher B, Gao S, Mäder E. Behaviour of strain-hardening cement-based composites under high strain rates. J Adv Concr Technol 2011;9(1):51–62.
[50] Chen M, Wang Y, Zhang T, Zhang M. Behaviour of structural engineered cementitious composites under dynamic tensile loading and elevated temperatures. Eng Struct 2023;280:115739.
[51] Zhao X, Li Q, Xu S. Contribution of steel fiber on the dynamic tensile properties of hybrid fiber ultra high toughness cementitious composites using Brazilian test. Constr Build Mater 2020;246:118416.
[52] Zhao X, Zou B, Wang M, Li H, Lou Z. Influence of free water on dynamic tensile behavior of ultra-high toughness cementitious composites. Constr Build Mater 2021;269:121295.
[53] Pyo S, El-Tawil S. Capturing the strain hardening and softening responses of cementitious composites subjected to impact loading. Constr Build Mater 2015;81:276–83.
[54] Gong T, Heravi AA, Alsous G, Curosu I, Mechtcherine V. The impact-tensile behavior of cementitious composites reinforced with carbon textile and short polymer fibers. Appl Sci 2019;9:4048.
[55] Tedesco JW, Ross CA, McGill PB, O'Neil BP. Numerical analysis of high strain rate concrete direct tension tests. Comput Struct 1991;40(2):313–27.
[56] Park JK, Kim S-W, Kim DJ. Matrix-strength-dependent strain-rate sensitivity of strain-hardening fiber-reinforced cementitious composites under tensile impact. Compos Struct 2017;162:313–24.
[57] Gao S, Gao R, Mu R, Zhu Y, Qi L. Effect of loading rate on mode I/mode II/mixed mode I–II fracture performance of engineered cementitious composites. Int J Solids Struct 2023;262-263:112052.
[58] Ismail MK, Hassan AAA, Lachemi M. Effect of fiber type on impact and abrasion resistance of engineered cementitious composite. Acids Mater J 2018;115(6):957–68.
[59] Hou W, Hu Y, Yuan C, Feng H, Cheng Z. Peridynamic simulation of dynamic fracture process of engineered cementitious composites (ecc) with different curing ages. Materials 2022;15(3494).
[60] Wu H, Zhu Z, Chen Y, Li H, Jiang W. Mechanical properties of short polypropylene fiber enhanced recycled concrete under cyclic compression. Struct Concr 2023;24:4751–66.
[61] Krahl PA, Carrazedo R, Debs MKE. Mechanical damage evolution in UHPFRC: Experimental and numerical investigation. Eng Struct 2018;170:63–77.
[62] Chen X, Huang Y, Chen C, Lu J, Fan X. Experimental study and analytical modeling on hysteresis behavior of plain concrete in uniaxial cyclic tension. Int J Fatigue 2017;96:261–9.
[63] Paschalis SA, Lampropoulos AP. Ultra-high-performance fiber-reinforced concrete under cyclic loading. Acids Mater J 2016;113(4):419–27.
[64] Wang C, Xiao J, Liu W, Ma Z. Unloading and reloading stress-strain relationship of recycled aggregate concrete reinforced with steel/polypropylene fibers under uniaxial low-cycle loadings. Cem Concr Compos 2022;131:104597.
[65] Singh M, Saini B, Devidas CH. Performance of cost effective engineered cementitious composite in exterior beam-column connections under cyclic loading. Struct Concr 2023;24:3692–707.
[66] Deng M, Pan J, Sun H. Bond behavior of deformed bar embedded in engineered cementitious composites under cyclic loading. Constr Build Mater 2019;197:164–74.
[67] Smedt MD, Vrijdaghs R, Steen CV, Verstrynge E, Vandewalle L. Damage analysis in steel fibre reinforced concrete under monotonic and cyclic bending by means of acoustic emission monitoring. Cem Concr Compos 2020;114:103765.
[68] Chen Y, He Q, Liang X, Chen Z, Li H. Experimental investigation on mechanical properties of steel fiber reinforced recycled aggregate concrete under uniaxial cyclic compression. Constr Build Mater 2023;387:131616.
[69] Tang Z, Cao B, Litina C, Afroughsabet V, Vlachakis C, Al-Tabbaa A. Development of novel self-healing strain-hardening cementitious composites (SH2CC) for dynamic cyclic loading conditions using mineral and polymer admixtures. Cem Concr Compos 2023;142:105172.
[70] Yang Z, Du Y, Liang Y, Ke X. Mechanical behavior of shape memory alloy fibers embedded in engineered cementitious composite matrix under cyclic pullout loads. Materials 2022;15:4531.
[71] Shan Z, Yu Z, Chen F, Li X, Gao J. Experimental investigation of mechanical behaviors of self-compacting concrete under cyclic direct tension. Materials 2019;12(1047).
[72] Chen Y, Xu L, Xuan W, Zhou Z. Experimental study on four-point cyclic bending behaviours of concrete with high density polyethylene granules. Constr Build Mater 2019;201:691–701.
[73] Li J, Li Y, Guo J, Wan M, Dong X. Structural Performance of Reinforced Strain Hardening Cementitious Composite Pipes during Cyclic Loading. IOP Conf Ser: Earth Environmenal Sci 2019;252:022041.
[74] Goel S, Singh SP. Fatigue performance of plain and steel fibre reinforced self compacting concrete using S–N relationship. Eng Struct 2014;74:65–73.
[75] Matsumoto T, Suthiwarapirak P, Kanda T. Mechanisms of Multiple Cracking and Fracture of DFRCC under Fatigue Flexure. J Adv Concr Technol 2003;1(3):299–306.
[76] Saucedo L, Yu RC, Medeiros A, Zhang X, Ruiz G. A probabilistic fatigue model based on the initial distribution to consider frequency effect in plain and fiber reinforced concrete. Int J Fatigue 2013;48:308–18.
[77] Huang B, Li Q, Xu S, Zhou B. Frequency effect on the compressive fatigue behavior of ultrahigh toughness cementitious composites: experimental study and probabilistic analysis. J Struct Eng 2017;143(8):04017073.
[78] Li Q, Huang B, Xu S, Zhou B, Yu RC. Compressive fatigue damage and failure mechanism of fiber reinforced cementitious material with high ductility. Cem Concr Res 2016;90:174–83.
[79] Leung CKY, Cheung YN, Zhang J. Fatigue enhancement of concrete beam with ECC layer. Cem Concr Res 2007;37:743–50.
[80] Khalil AE-H, Etman E, Atta A, Essam M. Behavior of RC beams strengthened with strain hardening cementitious composites (SHCC) subjected to monotonic and repeated loads. Eng Struct 2017;140:151–63.
[81] Zhu S, Zhang YX, Lee CK. Experimental investigation of flexural behaviours of hybrid engineered cementitious composite beams under static and fatigue loading. Eng Struct 2022;262:114369.
[82] Suthiwarapirak P, Matsumoto T, Kanda T. Multiple Cracking and Fiber Bridging Characteristics of Engineered Cementitious Composites under Fatigue Flexure. J Mater Civ Eng 2004;16(5):433–43.
[83] Medeiros A, Zhang X, Ruiz G, Yu RC, Velasco MdSL. Effect of the loading frequency on the compressive fatigue behavior of plain and fiber reinforced concrete. Int J Fatigue 2015;70:342–50.
[84] Lee MK, Barr BIG. An overview of the fatigue behaviour of plain and fibre reinforced concrete. Cem Concr Compos 2004;26:299–305.
[85] Zheng A, Wang S, Lu Y, Li S. Flexural Fatigue Behavior of Reinforced Concrete Beams Strengthened with Fiber-Reinforced Polymer Grid-Reinforced Engineered Cementitious Composite Matrix Composites. Acids Struct J 2022;119(6):205–19.
[86] Sherir MAA, Hossain KMA, Lachemi M. Structural Performance of Polymer Fiber Reinforced Engineered Cementitious Composites Subjected to Static and Fatigue Flexural Loading. polymers 2015;7:1299–330.
[87] Rutzen M, Volkmer D. Viscoelasticity and energy dissipation as indicators of flexural fatigue behavior in a ductile carbon fiber-reinforced cementitious composite. Int J Fatigue 2022;160:106839.
[88] Meng D, Lee C, Zhang Y. Flexural fatigue properties of a polyvinyl alcohol-engineered cementitious composite. Mag Concr Res 2019;71(21):1130–41.
[89] Liu L, Gao S, Xin J, Huang D. Effect of low-stress fatigue on the off-crack-plane fracture energy in engineered cementitious composites. Adv Civ Eng 2018;2018.
[90] Cachim PB, Figueiras JA, Pereira PAA. Fatigue behavior of fiber-reinforced concrete in compression. Cem Concr Compos 2002;24:211–7.
[91] Huang B, Li Q, Xu S, Zhang L. Static and fatigue performance of reinforced concrete beam strengthened with strain-hardening fiber-reinforced cementitious composite. Eng Struct 2019;199:109576.
[92] Bawa S, Singh SP. Analysis of fatigue life of hybrid fibre reinforced self-compacting concrete. Proc Inst Civ Eng – Constr Mater 2020;173(5):251–60.
[93] Guo W, Bao J, Zhang P, Yang J, Guo D, Tian Y. Self-healing behavior of strain-hardening cementitious composites with MgO-type expansive agent after drop weight impact loading. Constr Build Mater 2023;366:130235.
[94] Guo W, Tian Y, Wang W, Wang B, Zhang P, Bao J. Dynamic mechanical behavior of strain-hardening cementitious composites under drop weight impact loading. J Mater Res Technol 2023;23:5573–86.
[95] Yıldırım G, Khiavi FE, Anıl Ö, Sahin O, Sahmaran M, Erdem RT. Performance of engineered cementitious composites under drop-weight impact: effect of different mixture parameters. Struct Concr 2020;21:1051–70.

[96] Ismail MK, Hassan AAA, Lachemi M. Performance of self-consolidating engineered cementitious composite under drop-weight impact loading. J Mater Civ Eng 2019;31(3):04018400.
[97] Lin J, Song Y, Xie Z, Guo Y, Yuan B, Zeng J, Wei X. Static and dynamic mechanical behavior of engineered cementitious composites with PP and PVA fibers. J Build Eng 2020;29:101097.
[98] Ismail MK, Hassan AAA, Lachemi M. Effect of fiber type on impact and abrasion resistance of engineered cementitious composite. Acids Mater J 2018;115(6):957–68.
[99] Yang E-H, Li VC. Tailoring engineered cementitious composites for impact resistance. Cem Concr Res 2012;42:1066–71.
[100] Zhang Z, Qin F, Ma H, Xu L. Tailoring an impact resistant engineered cementitious composite (ECC) by incorporation of crumb rubber. Constr Build Mater 2020;262:120116.
[101] Ali MAEM, Soliman AM, Nehdi ML. Hybrid-fiber reinforced engineered cementitious composite under tensile and impact loading. Mater Des 2017;117:139–49.
[102] Lu C, Yu J, Leung CKY. Tensile performance and impact resistance of strain hardening cementitious composites (SHCC) with recycled fibers. Constr Build Mater 2018;171:566–76.
[103] Mahmoud MH, Afefy HM, Baraghith AT, Elnagar AB. Impact and static behavior of strain-hardening cementitious composites–strengthened reinforced concrete slabs. Adv Struct Eng 2020;23(8):1614–28.
[104] Máca P, Sovják R, Konvalinka P. Mix design of UHPFRC and its response to projectile impact. Int J Impact Eng 2014;63:158–63.
[105] Peng Y, Wu H, Fang Q, Liu JZ, Gong ZM. Residual velocities of projectiles after normally perforating the thin ultra-high performance steel fiber reinforced concrete slabs. Int J Impact Eng 2016;97:1–9.
[106] Wang S, Le HTN, Poh LH, Feng H, Zhang M. Resistance of high-performance fiber-reinforced cement composites against high-velocity projectile impact. Int J Impact Eng 2016;95:89–104.
[107] Xu S, Wu P, Zhou F, Jiang X, Chen B, Li Q. A dynamic constitutive model of ultra high toughness cementitious composites. J Zhejiang Univ-Sci A 2020;21(12):939–60.
[108] Xu S, Zhou F, Li Q, Chen B, Jiang X, Yin X, Wu P. Comparative study on performance of UHTCC and RPC thick panels under hard projectile impact loading. Cem Concr Compos 2021;122:104134.
[109] Wu P, Xu S, Li Q, Zhou F, Al-Mansour A, Zhao X. A plasticity-based dynamic constitutive model for ultra high toughness cementitious composites. Int J Impact Eng 2022;161:104086.
[110] Prakash A, Srinivasan SM, Rao ARM. Application of steel fibre reinforced cementitious composites in high velocity impact resistance. Mater Struct 2017;50(6).
[111] Kim G-Y, Choi J-I, Park S-E, Kim H, Lee Y, Lee BY. Response of UHPFRC and HDFRC under static and high-velocity projectile impact loads. Constr Build Mater 2018;188:399–408.
[112] Yin X, Li Q, Chen B, Xu S. An improved calibration of Karagozian & Case concrete/cementitious model for strain-hardening fibre-reinforced cementitious composites under explosion and penetration loadings. Cem Concr Compos 2023;137:104911.
[113] Liao Q, Xie X, Yu J. Numerical investigation on dynamic performance of reinforced ultra-high ductile concrete–ultra-high performance concrete panel under explosion. Struct Concr 2022;23:3601–15.
[114] Li J, Wu C, Hao H, Wang Z, Su Y. Experimental investigation of ultra-high performance concrete slabs under contact explosions. Int J Impact Eng 2016;93:62–75.
[115] Lan S, Lok T-S, Heng L. Composite structural panels subjected to explosive loading. Constr Build Mater 2005;19:387–95.
[116] Liao Q, Yu J, Xie X, Ye J, Jiang F. Experimental study of reinforced UHDC-UHPC panels under close-in blast loading. J Build Eng 2022;46:103498.
[117] Li Q, Chen B, Xu S, Zhou F, Yin X, Jiang X, Wu P. Experiment and numerical investigations of ultra-high toughness cementitious composite slabs under contact explosions. Int J Impact Eng 2022;159:104033.
[118] Chilvers J, Yang L, Lin X, Zhang YX. Experimental and numerical investigations of hybrid-fibre engineered cementitious composite panels under contact explosions. Eng Struct 2022;266:114582.
[119] Xu S, Chen B, Li Q, Zhou F, Yin X, Jiang X, Wu P. Experimental and numerical investigations on ultra-high toughness cementitious composite slabs subjected to close-in blast loadings. Cem Concr Compos 2022;126:104339.
[120] Zhong R, Zhang F, Poh LH, Wang S, Le HTN, Zhang M. Assessing the effectiveness of UHPFRC, FRHSC and ECC against high velocity projectile impact. Cem Concr Compos 2021;120:104013.
[121] Foglar M, Hajek R, Fladr J, Pachman J, Stoller J. Full-scale experimental testing of the blast resistance of HPFRC and UHPFRC bridge decks. Constr Build Mater 2017;145:588–601.
[122] Zhang Y, Li X, Wang Z, Jiang L, Leng Y, Zhang D. Shake table test on a five-story residential masonry building strengthened by engineered cementitious composites based on minimum disturbance. Eng Struct 2024;300:117227.
[123] Dong Z, Deng M, Dai J, Ma P. Diagonal compressive behavior of unreinforced masonry walls strengthened with textile reinforced mortar added with short PVA fibers. Eng Struct 2021;246:113034.
[124] Dong F, Li Z, Yu J, Jiang F, Wang H. Shaking-Table Test on a Two-Story Timber-Framed Masonry Structure Retrofitted with Ultra-High Ductile Concrete. J Struct Eng 2022;148(1):04021226.
[125] Zhang Y, Deng M, Dong Z. Seismic response and shear mechanism of engineered cementitious composite (ECC) short columns. Eng Struct 2019;192:296–304.
[126] Yuan F, Chen M, Pan J. Experimental study on seismic behaviours of hybrid FRP–steel-reinforced ECC–concrete composite columns. Compos B Eng 2019;176:107272.
[127] Xu L, Pan J, Cai J. Seismic performance of precast RC and RC/ECC composite columns with grouted sleeve connections. Eng Struct 2019;188:104–10.
[128] Bai C, Tian L, Yang P, Li T. Seismic behavior of concrete columns with ends transformed via perforated H-shaped steel and engineered cementitious composite. Soil Dyn Earthq Eng 2023;165:107725.
[129] Wu C, Pan Z, Su RKL, Leung CKY, Meng S. Seismic behavior of steel reinforced ECC columns under constant axial loading and reversed cyclic lateral loading. Mater Struct 2017;50(78).
[130] Dong F, Yu J, Zhan K, Li Z. Seismic fragility analysis of two-story ultra-high ductile cementitious composites frame without steel reinforcement. Adv Struct Eng 2020;23(11):2373–87.
[131] Abbas AA, Mohsin SMS, Cotsovos DM. Seismic response of steel fibre reinforced concrete beam–column joints. Eng Struct 2014;59:261–83.
[132] Hou L, Xu R, Chen D, Xu S, Aslani F. Seismic behavior of reinforced engineered cementitious composite members and reinforced concrete/engineered cementitious composite members: A review. Struct Concr 2020;21:199–219.
[133] Huang L, Xu L, Chi Y, Xu H. Experimental investigation on the seismic performance of steel–polypropylene hybrid fiber reinforced concrete columns. Constr Build Mater 2015;87:16–27.
[134] Li W, Ye H, Sun L. Experimental study on seismic behavior of T-shaped steel fiber reinforced concrete columns. Struct Concr 2023;24:612–33.
[135] Qudah S, Maalej M. Application of Engineered Cementitious Composites (ECC) in interior beam–column connections for enhanced seismic resistance. Eng Struct 2014;69:235–45.
[136] Yu J, Dong Z, Yu J, Liu F, Ye J, Dong F. Dynamic Response of Masonry Walls Strengthened with Engineered Cementitious Composites under Simulated Debris Flow. J Struct Eng 2022;148(9):04022113.
[137] Chen X, Zhang Y, Wang Z, Yu J, Skalomenos K, Xu Q. Shaking table tests on a 5-storey unreinforced masonry structure strengthened by ultra-high ductile cementitious composites. J Build Eng 2022;54:104635.
[138] Deng M, Dong Z, Wang X, Zhang Y, Zhou T. Shaking table tests of a half-scale 2-storey URM building retrofitted with a high ductility fibre reinforced concrete overlay system. Eng Struct 2019;197:109424.
[139] Lei B, Li X, Guo Y, Qu F, Zhao C, Tam V, Wu V, Li W. Recycling of copper tailing as filler material in asphalt paving mastic: A sustainable solution for mining waste recovery. Case Stud Constr Mater 2024;20:e03237.
[140] Lin X, Castel A, Deng Z, Dong B, Zhang X, Zhang S, Li W. Effect of crystalline admixtures on shrinkage and alkali-silica reaction of biochar-cementitious composites. Dev Built Environ 2024;18:100456.
[141] Lu D, Qu F, Punetha P, Zeng X, Luo Z, Li W. Graphene oxide nano-engineered recycled aggregate concrete for sustainable construction: A critical review. Dev Built Environ 2024;18:100444.
[142] Yang K, Tang Z, Li W, Wu H, Ma G, Xiang Y, Xie Y, Long G. A systematic review on the evaluation methods for the flexural toughness of cement-based materials: From classification analysis to case study. J Build Eng 2024;93:109855.